Quaternary Science Reviews 112 (2015) 86–108

Contents lists available at ScienceDirect

Quaternary Science Reviews

journal homepage: www.elsevier.com/locate/quascirev

Discriminating between subglacial and proglacial lake sediments: an example from the Dänischer Wohld Peninsula, northern Germany

Stephen J. Livingstone [a, *], Jan A. Piotrowski [b], Mark D. Bateman [a], Jeremy C. Ely [a], Chris D. Clark [a]

[a] Department of Geography, University of Sheffield, Sheffield S10 2TN, United Kingdom
[b] Department of Geoscience, Aarhus University, DK-8000 Aarhus, Denmark

ARTICLE INFO

Article history:
Received 1 November 2014
Received in revised form
25 January 2015
Accepted 28 January 2015
Available online

Keywords:
Subglacial lake
Proglacial lake
Ice Sheet
Sedimentology
Optically Stimulated Luminescence dating
Northern Germany

ABSTRACT

Subglacial lakes are common features of contemporary ice masses. However, they are rarely identified in the geological record. This is due to the difficulty in discriminating between subglacial and proglacial lake sediments; a proglacial origin is typically preferred as the 'simplest' explanation. We hypothesise that numerous deposits currently interpreted to record proglacial lake sedimentation may actually have a subglacial origin. Here we try and find ways of distinguishing proglacial from subglacial lake sediments by investigating three sites along the Dänischer Wohld Peninsula, northern Germany, which have been interpreted to record both proglacial and subglacial sedimentation. We identify two major phases of ice activity and associated lake formation during the Late Weichselian glaciation. (1) Proglacial lake formation at ~23 ka in front of the advancing Baltic Ice Stream. This lake was subsequently overridden and the sediments glaciotectonised as ice continued to advance to its maximum extent. (2) Retreat of ice back into the Baltic Basin at ~19 ka and formation of a proglacial lake that persisted for ~4 ka. We suggest that subglacial lake activity may have occurred at two of the sites between 23 and 19 ka. This is based on the presence of aggrading sediment deposits characterised by stratified/laminated diamictons and interbedded tabular to channelized sorted sediments, the juxtaposition of relatively undeformed waterlain sediment and subglacial till, absence of glaciotectonic thrusting and folding or of fining/coarsening successions and the geomorphic association with tunnel valleys to the south of the study area. The style of sedimentation and deformation provided the greatest insight into the discrimination of proglacially vs subglacially deposited glaciolacustrine sediments. The luminescence signal palaeodose distributions also offers a potentially powerful means of fingerprinting sediment transport pathways of young glacial systems.

1. Introduction

Glaciolacustrine sediments are commonly observed in the geological record and have classically been interpreted to record proglacial (ice-marginal or ice-fed) lake formation (e.g. Rust and Romanelli, 1975; Eyles, 1987; Eyles et al., 1989; Larsen et al., 2006; Livingstone et al., 2010; Carrivick and Tweed, 2013). If the geographic context for these sediments in relation to a former ice margin is suitable for lake impoundment, or where other lines of evidence exist – such as lake shorelines and/or deltas – then such an interpretation is robust. It is common, however, to find glaciolacustrine sediments without ancillary support for a proglacial origin, and we raise the question; in some of these cases could the sediments have been deposited in a subglacial lake? We suggest that breaking the automatic interpretation from glaciolacustrine sediments to the existence of a proglacial lake is timely because subglacial lakes are now known to be commonplace beneath contemporary ice masses (e.g. Wright and Siegert, 2011), and are predicted to exist beneath palaeo-ice sheets (Evatt et al., 2006; Livingstone et al., 2013). Given that they must surely have existed, it is sensible therefore to hypothesise that many glaciolacustrine sediments previously interpreted as proglacial might actually have a subglacial origin. If we can distinguish the signature of subglacial lake sediments we could glean important spatial and geological evidence on: (i) meltwater drainage, ice flow and ice streams; (ii) their relation to palaeo-floods, ice dynamics and sub-

* Corresponding author.
E-mail address: s.j.livingstone@sheffield.ac.uk (S.J. Livingstone).

http://dx.doi.org/10.1016/j.quascirev.2015.01.030

Milankovitch-scale climate events; and (iii) long-term Quaternary climate change (Livingstone et al., 2012).

Despite recent attempts to formulate diagnostic criteria based on our current knowledge of subglacial lake processes (e.g. Bentley et al. 2011; Livingstone et al. 2012; Ravier et al., 2014a), there is still no incontrovertible method for distinguishing their geological signature from that of proglacial lakes and therefore for demonstrating their former existence. So, despite putative examples of palaeo-subglacial lakes (e.g. Gjessing, 1960; McCabe and Ó Cofaigh, 1994; Rebesco et al., 1998; Munro-Stasiuk, 1999; van Rensbergen et al., 1999; Christoffersen et al., 2008), a proglacial lake origin is typically preferred as the 'simplest' interpretation for glaciolacustrine sediments.

We explore this conundrum using the glacigenic succession of the Dänischer Wohld Peninsula, northern Germany, in an attempt to advance our skill in the discrimination of proglacially vs subglacially deposited glaciolacustrine sediments. The sediments exposed along this Peninsula have been variously interpreted to record deposition in subglacial and proglacial lake environments (Piotrowski, 1992, 1994a,b, 1997; Hart et al., 1996, 1997; Piotrowski et al., 1997; Piotrowski and Tulaczyk, 1999). Our aim is to test these two conflicting models using a range of techniques, including geomorphological mapping, sedimentological and stratigraphic investigations, and Optically Stimulated Luminescence (OSL) dating.

2. Location and glacial context

The Dänischer Wohld Peninsula is part of Schleswig–Holstein, northern Germany and is located between deeply incised bays of the southwestern Baltic Sea at Eckernförde and Kiel (Figs. 1 and 2). An up to 25 m high sea cliff has exposed a remarkable record of intercalated glacigenic facies deposited during the Weichselian glaciation subdivided by Piotrowski (1996) into the lower and upper sedimentary complexes. The succession is interpreted to record either: (1) a single advance of ice out of the Baltic Basin, which

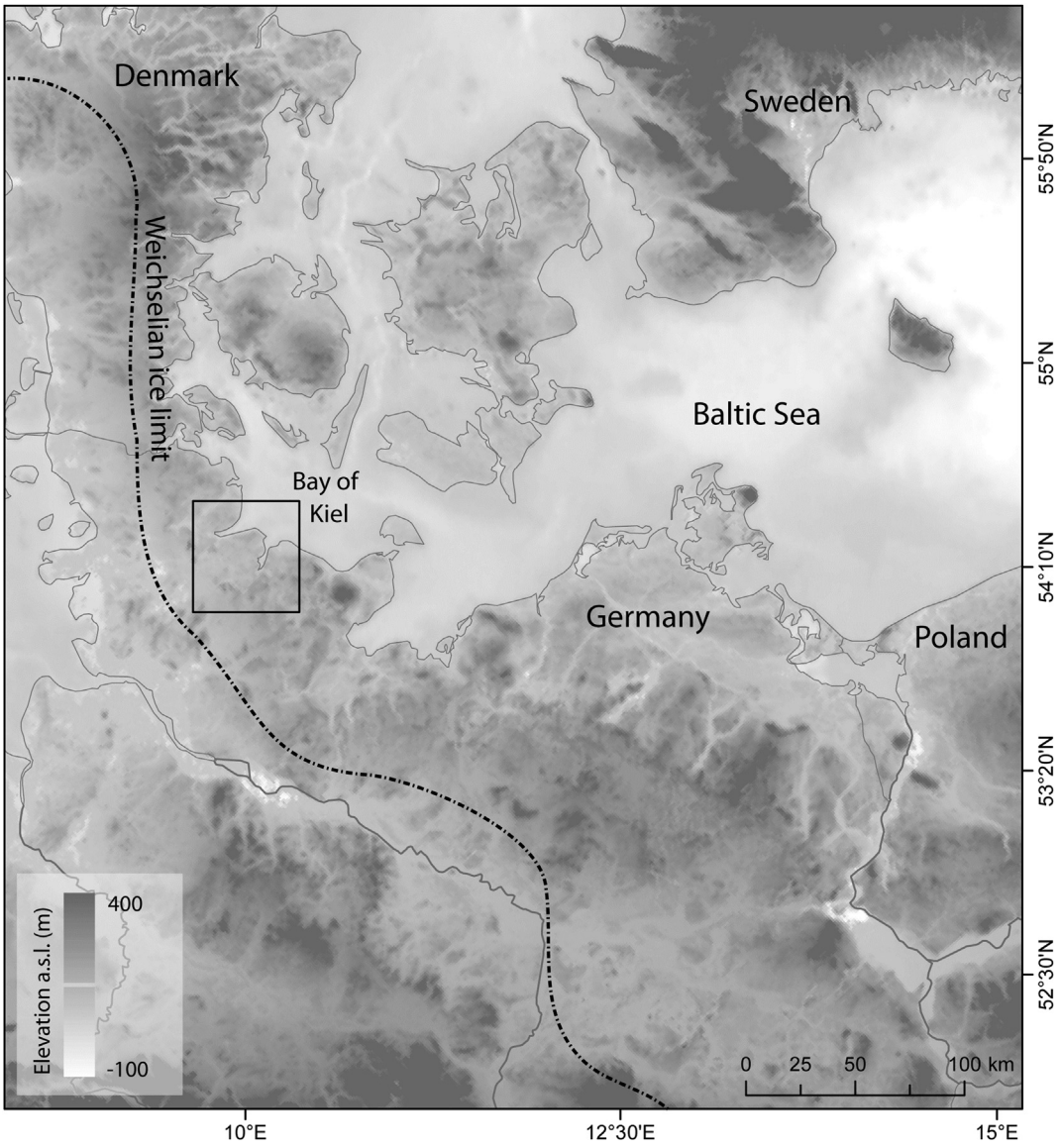

Fig. 1. Location map of the Dänischer Wohld Peninsula, northern Germany. Inset box relates to Fig. 2.

dammed and subsequently overrode a proglacial lake (Piotrowski, 1992, 1994a; Piotrowski et al., 1997); (2) a series of readvances during overall glacial retreat, with subglacial deformation occurring during each advance and glaciolacustine sedimentation during each retreat (Hart et al., 1996, 1997); or (3) sedimentation in a subglacial lake basin that periodically drained in tunnel valleys through a permafrost seal (Piotrowski, 1994b, 1997; Piotrowski and Tulaczyk, 1999). These sediments comprise part of an extensive succession of Quaternary deposits that reach up to 200 m thick (Piotrowski, 1994b).

Retreat of the Scandinavian Ice Sheet and development of ice-free conditions in northern Germany and Denmark after 29 ka BP was followed by renewed growth of the Baltic ice streams to their maximum limits between 25 and 22 ka BP (Houmark-Nielsen and Kjaer, 2003; Jørgensen and Piotrowski, 2003; Larsen et al., 2009; Sommer and Benecke, 2009; Houmark-Nielsen, 2010; Ukkonen et al., 2011), terminating some 50 km to the south and 25 km to the west of the study area. Stratigraphic investigations have identified five glacial fluctuations during this expansion, the first four of which took place south of the study area, which remained ice covered (Stephan and Menke, 1977; Stephan et al., 1983; Prange, 1987, 1990). After the fourth advance ice retreated offshore of the Dänischer Wohld Peninsula before re-advancing out of the eastern Baltic Sea (over the study site) and terminating several kilometres south of the present shoreline (Mecklenburg Phase, Young Baltic Advance; Stephan, 1995, 2001). Final retreat of ice out of northern Germany is thought to have occurred after ~19 ka BP (Lüthgens et al., 2011; Houmark-Nielsen et al., 2012), and possibly as late as ~15 ka (Preusser, 1999), although this conflicts with deglacial chronologies further north, which suggest the ice margin reached southern Sweden between 18 and 16 ka BP (Lundqvist and Wohlfarth, 2001; Anjar et al., 2014).

3. Methods

3.1. Glacial geomorphology mapping

Glacial geomorphological mapping of the Schleswig–Holstein region of northern Germany involved the recognition and interpretation of glacial landforms from NEXTMap digital surface model (DSM) data (Fig. 2a). This is a 5 m resolution DSM derived using airborne Interferometric Synthetic Aperture Radar (IFSAR) imagery (http://www.intermap.com/data/nextmap). Mapping was carried out manually using on-screen digitisation. Vectors were used to digitise channels, moraine ridges and eskers, and points used to digitise hummocky moraine. Long profiles along channels were extracted in order to assess a subglacial vs proglacial origin.

3.2. Sedimentology

Sedimentological and stratigraphic investigations were carried out using a range of macro- and micro-scale techniques at three sites along the Dänischer Wohld Peninsula (Fig. 2). Sections were logged and information on sedimentary structure, bed geometry, texture, sorting and colour (Munsell) used to characterise lithofacies (based on the nomenclature of Evans and Benn, 2004). Scaled section sketches were drawn from a series of overlapping photographs so that the lateral extent of the lithofacies could be assessed. At 16 sites clast macro-fabrics were measured using the A-axes of stones with lengths ranging from 1 to 10 cm and A/B axial ratios of at least 1.5/1 ($n = 30$ at each fabric site). At 15 sites sediment samples were collected for the analysis of grain-size distribution (fraction $\leq$2 mm) and lithological components (fine-gravel fraction). In each sample, the lithological composition was determined on a minimum of 300 grains in the 2–4 mm size fraction whereby rocks are subdivided into stable

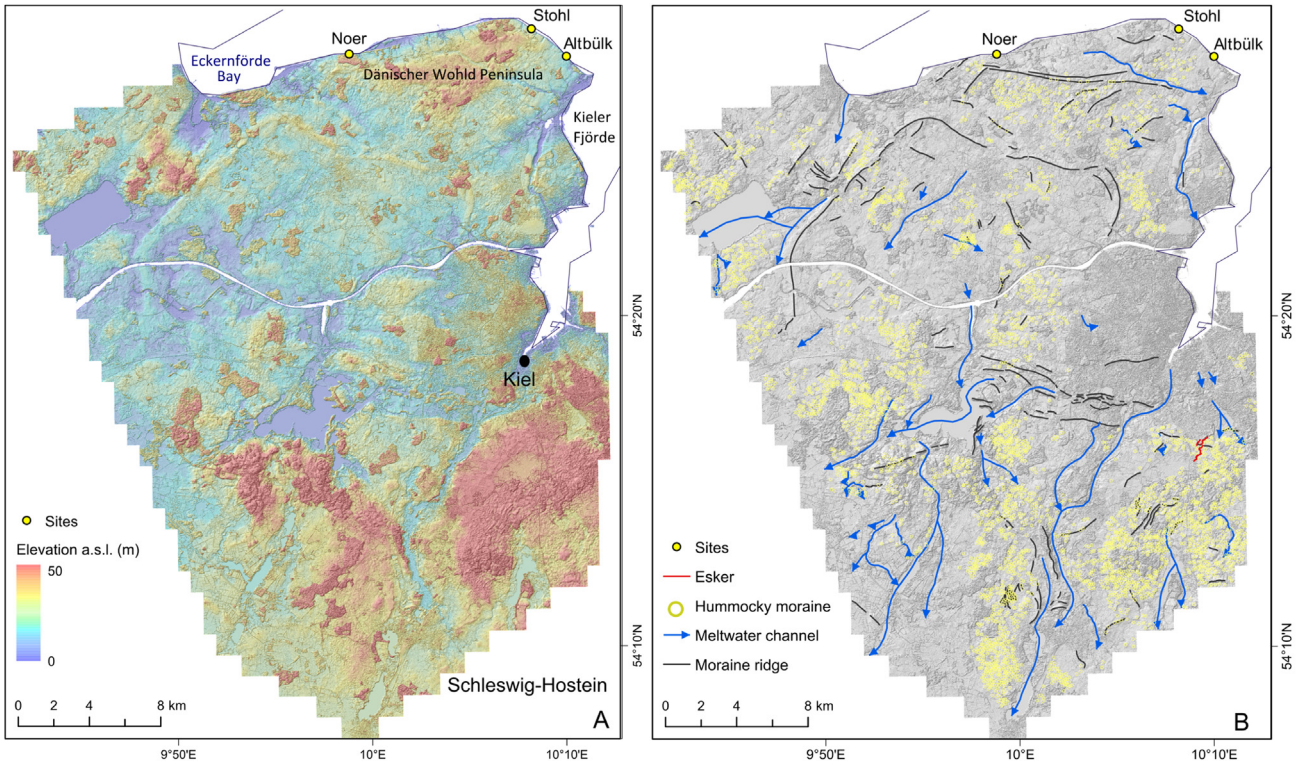

Fig. 2. Glacial geomorphology (A) and mapping (B) from 5 m NETXMap data of tunnel valleys, moraine, eskers and hummocky moraine in the Dänischer Wohld Peninsula of Schleswig–Holstein, northern Germany. Panel A displays the elevation and hillshaded DSM and panel B displays the hillshade and mapping results.

components (red crystalline rocks, light-coloured crystalline rocks, dark-coloured crystalline rocks, quartz, chert, and sandstone) and unstable components (Cretaceous and Danian chalk, Paleozoic limestone, calcareous sedimentary rocks, opal chert, and other lithologies) (Kronborg, 1986). The counting results are presented separately for stable and unstable lithologies whereby the sum of stable components gives 100% to enable sample-to-sample comparison not biased by weathering. At four sites undisturbed, oriented samples were collected in large Kubienä boxes (10 × 5.5 × 4 cm) for thin section production to investigate micromorphological characteristic of the deposits. Standard techniques were used for the impregnation and preparation of the thin sections (e.g. van der Meer, 1996).

3.3. Optically Stimulated Luminescence dating

OSL dating is a potentially powerful tool for deciphering between subglacial and proglacial lake sediments because sediment entering a subglacial lake is not exposed to sunlight and so the bleaching history will be different to that of a proglacial lake (Fig. 3). Fig. 3b–d displays possible D_e distributions that might be expected for subglacial and proglacial environments. The luminescence signal in a proglacial environment will vary depending upon its depositional pathway (Fig. 3a), typically resulting in a skewed distribution indicative of partial bleaching (Fig. 3b) (e.g. Fuchs and Owen, 2008). In contrast, subglacial lake sediments will retain an inherited signature of the event prior to deposition. Thus we might expect erroneously old ages related to the inherited signal from previous depositional events (Fig. 3c) or from grains with a saturated OSL signal derived from comminuted bedrock (Fig. 3d). The distribution may be less peaky or even multi-modal because it is derived from an amalgam of sediment that has been eroded or cannibalised, before being transported and deposited by ice. In the Fig. 3c scenario grains are sourced from a former proglacial lake during initial ice-advance. The reworking of sediment characterised by different depositional histories is also not expected to produce ages in the correct stratigraphic order. However, where proglacial lake sediments have been poorly bleached, or in regions where the bedrock has quartz with poor OSL characteristics (e.g. Alexanderson and Murray, 2012) it may be difficult to distinguish between proglacial and subglacial environments.

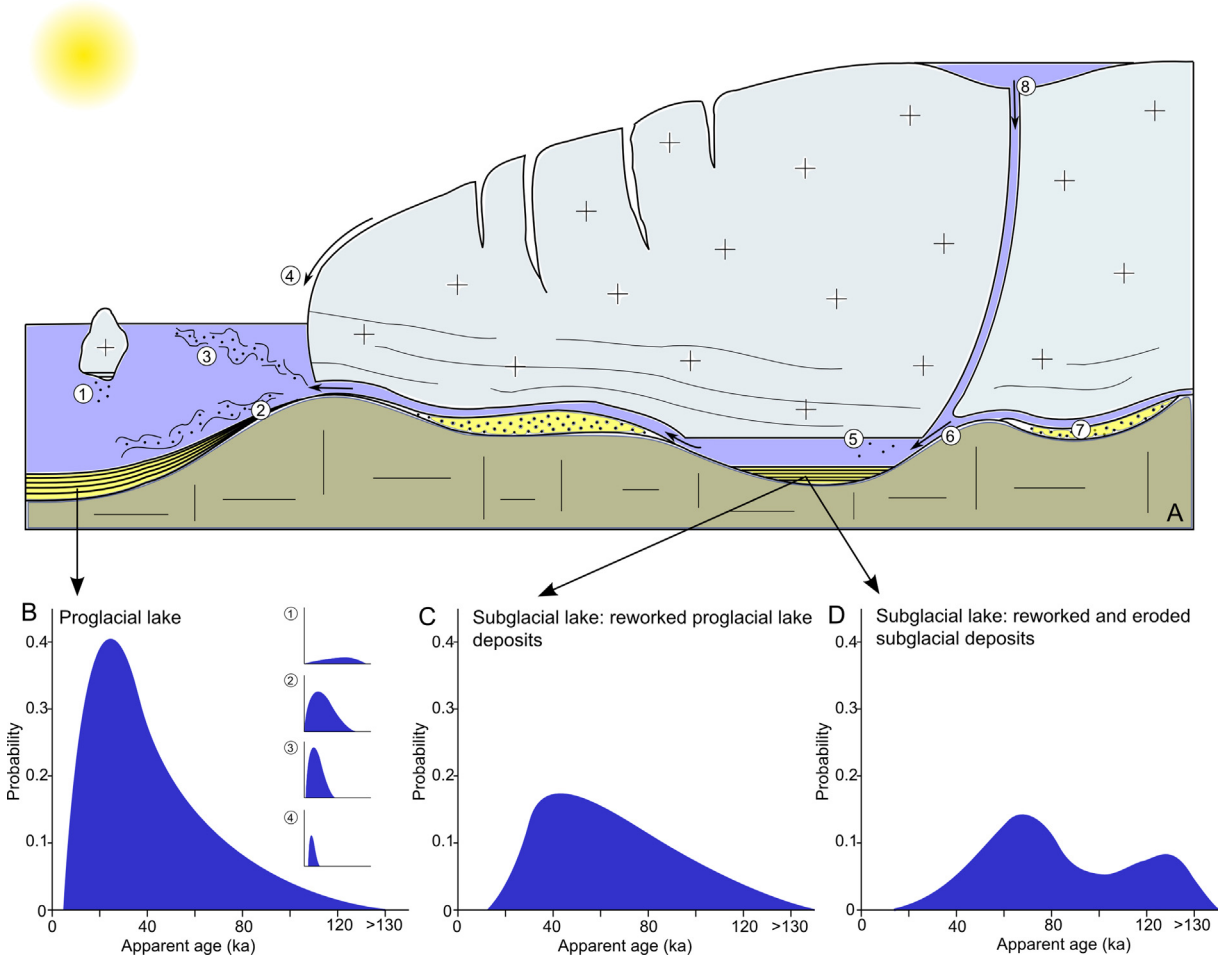

Fig. 3. A. Cartoon of sediment-transport pathways into subglacial and proglacial lake environments. 1 – Iceberg rainout; 2 – turbidity currents, underflows and gravity flows; 3 – sediment overflows (buoyant plumes); 4 – supraglacial drainage; 5 – melt-out of debris-rich ice; 6 – erosion of bedrock (meltwater drainage, plucking, abrasion, quarrying); 7 – reworking and deformation of subglacial and inherited sediments; 8 – supraglacial drainage. B: Probability density function plot displaying a hypothesised D_e distribution for deposition of the glaciolacustrine sediments from the Dänischer Wohld Peninsula in a proglacial lake. Insets 1-4 relate to numbers 1-4 in panel A. Assumed fully bleached burial age is 20 ka. Apparent ages of >130 ka relate to saturated grains. C and D: Probability density function plot displaying hypothesised age replicate distributions for deposition of the glaciolacustrine sediments from the Dänischer Wohld Peninsula in a subglacial lake. In scenario C there is a dominant component of sediments reworked from a former proglacial lake (note the older average age associated with this inherited signature and the greater number of saturated grains). In scenario D most of the sediment has been derived from reworked subglacial sediments and eroded bedrock. Note the high number of saturated grains associated with very old comminuted bedrock. Differences between comminuted geological age sediments and reset sediment should be great. Differences between older sediment mixed with reset sediments may or may not be great depending on the time elapsed between the two events.

Seven samples of sand collected from Noer and Altbülk were dated by the Optically Stimulated Luminescence (OSL) method to establish the timing of sediment burial and to try and elucidate the environmental context of deposition. All luminescence samples were collected from freshly exposed sections using opaque plastic tubes and immediately sealed with opaque end caps and tape to avoid light contamination. These were transported to and prepared under low-intensity red lighting at the Sheffield Luminescence Laboratory. All samples were prepared to extract and clean quartz. Carbonates and organic materials were removed using 1 M HCl acid and 30% H_20_2 respectively. Each sample was dry-sieved to isolate sand in the range 90–180 μm. A density separation using sodium polytungstate (specific gravity of 2.7 g cm^{-3}) was used to remove heavy minerals and the resultant extract was etched with 40% HF acid for 45 min to remove contaminated feldspars and surface coatings from quartz. Re-sieving at the lower size range was used to separate quartz from any residual feldspars and the purity was tested using infra-red stimulated luminescence.

OSL measurements were carried out both at the single aliquot and single grain level which has been successfully applied to glacial sediments elsewhere (e.g. Bateman et al., 2011). Single aliquot OSL measurements were conducted on 9.6 mm discs, with quartz deposited as a 2 mm diameter monolayer in the centre of the disc. Single grain measurements carried out with grains mounted on discs with 100 pits of 300 μm diameter arranged in a 10 × 10 grid. All measurements were carried out on a TL-DA-15 Risø automated luminescence reader equipped with a Hoya U340 filter (7.5 mm for single aliquot, 2.5 mm for single grain). OSL Stimulation was provided by blue diodes emitting at 470 nm for single aliquots and Nd:YVO_4 laser for single grain OSL measurements.

Single grain and single aliquot D_e values were derived using the single aliquot regeneration (SAR) protocol (Murray and Wintle, 2000), using four regeneration points and a recycling dose (Supplementary Fig. 1). The preheat temperature of 160 °C was determined experimentally using a dose-recovery plateau test on standard aliquots from one of the samples (Murray and Wintle, 2003). At this preheat temperature dose recovery was within 5% of unity (n = 3) and showed good recycling values (<10%) (Supplementary Fig. 2). Twenty-four replicates for each sample were measured at the single aliquot level. For single aliquot D_e calculations, aliquots were only accepted if: (i) the recycling ratio was within 10% of unity; recuperation was <5%; D_e error was <20%; the naturally-acquired OSL was significantly above background; and SAR regeneration points could be fitted adequately by a growth curve. For single grain D_e calculations, grains were accepted on the same basis as above except the recycling ratio relaxed to within 20% of unity to account for poorer signal to noise ratios. Also for single grain measurements, to minimise the influence of any slow component we adopted the method of Cunningham and Wallinga (2010) using a background integral that immediately followed and was 2.5× the initial signal. Finally, single grain measurements were only accepted if their OSL sensitivity exceeded 20 ct Gy^{-1} to avoid D_e scatter derived from dim grains (Rhodes, 2007). This final step significantly reduced the number of accepted grains per sample (on average only 36% accepted).

Analyses were initially carried out using single aliquots because this returns a good signal-to-noise ratio and where only a few bright grains are contributing to the OSL signal 2 mm diameter aliquots can be considered almost single grain measurements (Medialdea et al., 2014). However, replicate single aliquot D_e results showed appreciable scatter. Subsequent analysis of single grain data showed contributions were not dominated by a single grain and that the single aliquot approach was failing to reveal the true palaeo-dose (D_e) variability in resetting within samples. Obscuration of true D_e variability at the single aliquot level has been reported elsewhere stemming from the measurement of many grains

Table 1
OSL related data for sampled sites Dänischer Wohld Peninsula, northern Germany.

Sample details		Dose rate data					Single aliquot OSL measurement data			Single grain OSL measurement data				Age (ka)[c]
Lab code	Depth (m)	Alpha (μGy a^{-1})	Beta (μGy a^{-1})	Gamma (μGy a^{-1})	Cosmic dose rate (μGy a^{-1})	Total dose rate (μGy a^{-1})	n	OD (%)	CAM D_e (Gy)	n[a]	OD (%)	Skew	D_e (Gy)[b]	
Altblück														
Shfd12083	1.0	39 ± 7	1439 ± 119	606 ± 39	184 ± 9	2267 ± 126	27	23	34.75 ± 1.08	76 (26)	34	1.26	CAM 34.52 ± 2.17	**15.2 ± 1.28**
Shfd12081	3.3	36 ± 8	1479 ± 123	645 ± 41	120 ± 6	2280 ± 130	35	28	44.57 ± 1.44	72 (31)	48	1.57	CAM 38.10 ± 2.95	**16.7 ± 1.61**
													MAM 25.20 ± 4.19	11.1 ± 1.94
													FMM (1) 25.08 ± 2.94 (34)	11.0 ± 1.43
													FMM (2) 47.85 ± 4.23 (53)	21.0 ± 2.21
													FMM (3) 96.02 ± 15.18 (13)	42.1 ± 7.08
Shfd12082	4.3	39 ± 8	1333 ± 108	672 ± 43	136 ± 7	2179 ± 117	31	43	52.26 ± 3.54	60 (20)	57	4.38	CAM 39.97 ± 4.28	**18.3 ± 2.20**
													MAM 20.52 ± 4.51	9.42 ± 2.10
													FMM (1) 23.65 ± 3.29 (31)	10.9 ± 1.62
													FMM (2) 53.30 ± 4.08 (61)	24.5 ± 2.00
Shfd12079	5.0	24 ± 5	1205 ± 102	560 ± 36	104 ± 5	1812 ± 108	38	55	39.39 ± 3.08	61 (26)	54	3.52	CAM 37.67 ± 3.24	19.9 ± 1.85
													MAM 25.51 ± 6.09	13.5 ± 3.31
													FMM (1) 35.95 ± 2.83 (61)	**19.0 ± 1.85**
													FMM (2) 71.21 ± 8.79 (27)	37.6 ± 5.10
Noer														
Shfd12084	6.5	17 ± 5	839 ± 75	535 ± 34	110 ± 6	1483 ± 83	32	37	37.24 ± 1.75	52 (17)	35	0.53	CAM 27.46 ± 1.65	**18.52 ± 1.5**
Shfd12086	5.5	17 ± 2	830 ± 74	612 ± 39	110 ± 6	1569 ± 84	34	30	46.89 ± 2.03	49 (14)	54	2.34	CAM 39.64 ± 3.62	25.3 ± 2.68
													MAM 33.90 ± 3.53	21.6 ± 2.53
													FMM (1) 36.20 ± 3.11 (74)	**23.1 ± 2.33**
													FMM (2) 111.8 ± 15.6 (26)	71.3 ± 10.6
Shfd12085	5.0	33 ± 7	1096 ± 90	558 ± 35	104 ± 5	1797 ± 97	24	29	48.25 ± 1.19	60 (14)	60	0.99	CAM 41.57 ± 3.14	**23.1 ± 2.15**

[a] n equals number of aliquots measured and meeting initial acceptance criteria. Number in parenthesis indicates number of accepted grains once additional sensitivity criteria applied.

[b] Different models used to calculate single D_e from replicate D_e data. CAM is the Central Age Model, MAM is the Minimum Age Model and FMM the Finite Mixture Model. Note results for FMM D_e components exclude those representing less than 10% of the measured data with proportion of data represented by a given component indicated in parenthesis.

[c] Age in bold indicated preferred age based on D_e replicate data and stratigraphy (See text for details).

simultaneously to produce an average luminescence signal (e.g. Arnold and Roberts, 2009; Bateman et al., 2014). We therefore focus on the single grain results in this paper.

Dose rates were determined from field measurements made with an EG&G Micronomad field gamma-spectrometer to derive the gamma dose rate combined with laboratory based inductively-coupled plasma mass spectrometry (ICP-MS) measurements to determine the beta dose rate. The cosmic dose rate was determined following published algorithms (Prescott and Hutton, 1994). The total dose rates were attenuated for sediment size and palaeomoisture contents, with the latter based on present-day values determined at the time of sampling with an absolute error of 5%.

As was expected from the depositional contexts, the majority of samples analysed in this study were significantly overdispersed (OD), skewed and/or multimodal, indicative of partial bleaching which resulted in a range of D_e values within each sample (Table 1). For age calculation purposes, to derive single D_e values for each sample, replicate D_e data was analysed through a variety of age models. Where sample D_e distributions were unimodal, normally distributed and with a low OD, the sample was considered to be well bleached and of a single age. In such cases it was appropriate to use the Central Age Model (CAM; Galbraith and Green, 1990) to calculate a single D_e value for age calculation, once outliers (defined as falling outside the 1.5 times the fourth spread from the median; Hoaglin et al., 1983) were discarded. Where sample D_e distributions were skewed, with a high OD, then the sample was considered partial bleached with some grains carrying an antecedent geological signal masking the true burial age. In such cases an age model targeting the lowest component of D_e data, such as the minimum age model (MAM; Galbraith et al., 1999), was more appropriate. Where sample D_e distributions were non-normally distributed, multi-modal and with a high OD, the sample could be interpreted as partially bleached, and/or post-depositionally disturbed and/or having multiple age components (Bateman et al., 2003, 2007, 2014). In such cases the finite mixture model (FMM; Galbraith and Green, 1990; Galbraith et al., 1999) was considered. Critical to the latter was the use of an appropriate sigma-b value. This was experimentally determined for this study on the basis of a dose-recovery test which showed only that a sigma-b value of 0.2 was required to recover a dose within unity using FMM. Where FMM was applied for age calculation purposes only the FMM component representing more than 10% of the dataset were considered.

4. Glacial geomorphology

Geomorphological mapping of glacial landforms reveals a complex pattern of terminal and hummocky moraine bisected by or blanketing a network of ~6 km spaced channels (Fig. 2). These channels are up to 4 km wide (average ~500 m) and 200 m deep, and rise up the adverse slope from the Baltic Basin towards the Saalian highlands forming part of a wider network of channels that terminate close to or at the former ice-margin (Fig. 1, Ehlers and

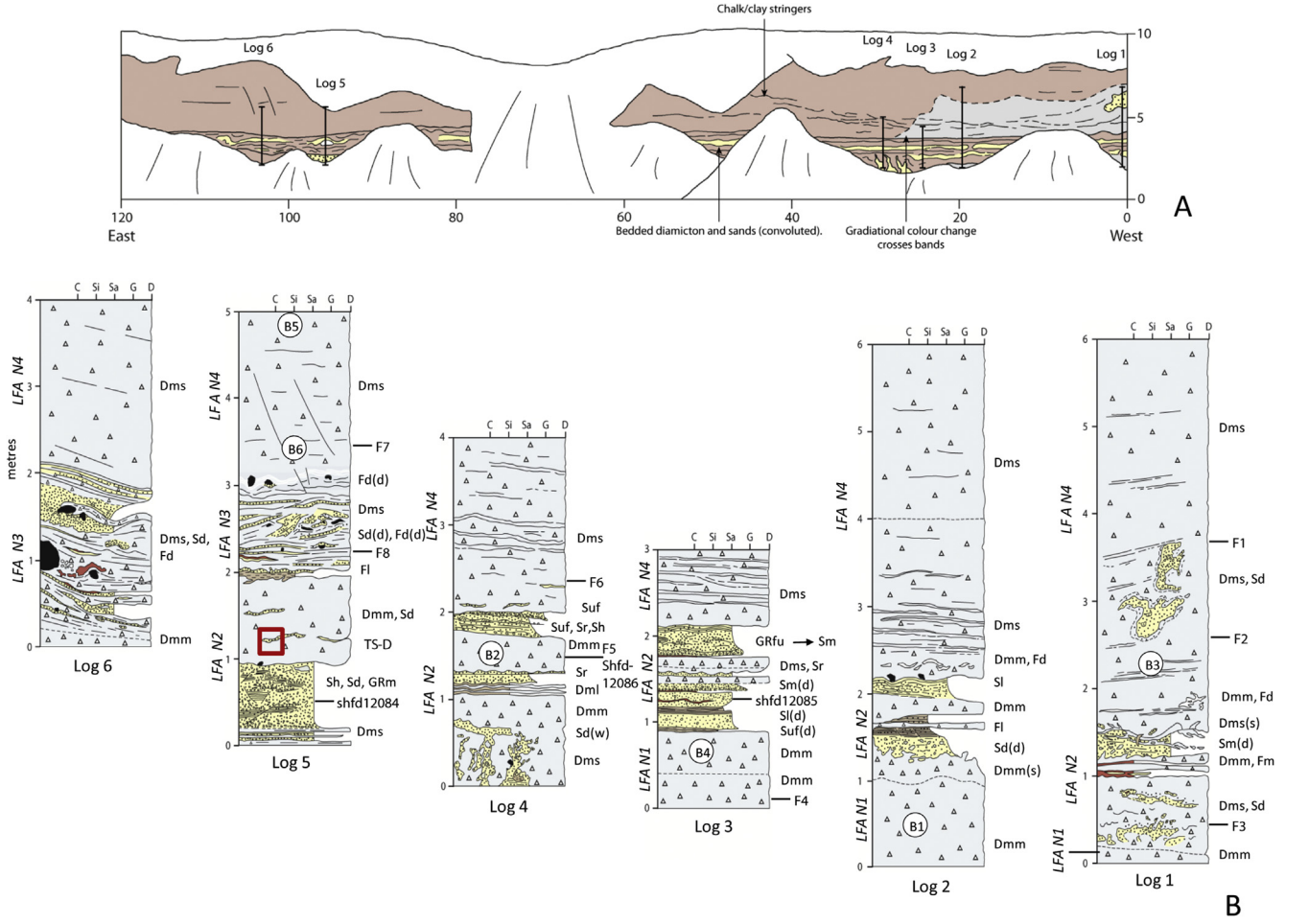

Fig. 4. Stratigraphic logs at Noer. White areas in the section log (A) were not exposed. The location of thins sections (TS), bulk samples for clast lithology and particle size (B), OSL samples (shfd code) and fabrics (F) are illustrated on the vertical logs. Lithofacies codes are based upon those of Evans and Benn (2004) (see Table 2 for classification of lithofacies and lithofacies associations).

Wingfield, 1991). At the Dänischer Wohld Peninsula the channels are preferentially aligned with the deeply incised Eckernförde Bay and Kieler Förde (Fig. 2b). A number of smaller <1 km wide channels are also observed, both associated with the larger channels and as isolated features (Fig. 2).

The spatial association with the former ice-margin, up-slope thalwegs, infilling by glacigenic sediments and partial burial by hummocky and terminal moraine has allowed the large channels to be interpreted as subglacially eroded tunnel valleys (see also Ehlers and Wingfield, 1991; Piotrowski, 1994b, 1997) and the smaller channels as subglacial meltwater channels. An extensive borehole investigation of the infilled Bornhöved tunnel valley south of Kieler Förde by Piotrowski, 1994b reveals it to be a polygenetic feature eroded over multiple glaciations. Sandur deposits in front of the Bornhöved tunnel valley comprising large numbers of well-rounded boulders up to 20 cm diameter indicate meltwater drainage by high-energy outbursts.

5. Sedimentology and stratigraphy

5.1. Noer

We examined and recorded exposed glacigenic sediments along 120 m of the east-west orientated, 9–12 m high Baltic Sea cliff near Noer (54°28.075′ N, 9°59.301′ W). Six sedimentary logs were recorded along the length of the exposure (Fig. 4), which is predominantly composed of stratified diamicton, interbedded with sorted sand and mud that volumetrically exceeds the diamicton in the middle third of the exposure (Table 2). Towards the cliff-top the diamicton becomes increasingly massive and can be confidently traced across all six logs. There is a noticeable absence of erosional contacts between sedimentary facies, and striated and faceted clasts are rare.

5.1.1. Lithofacies Association 1 (LFA N1; diamicton)

The lowermost lithofacies association (LFA), N1, is >1 m thick and comprises a dark grey (5Y 4/1), massive, matrix-supported diamicton (Dmm) that is clast poor and has a fissile appearance. A single fabric (F4) reveals a moderately strong ($S_1 = 0.71$), spread-unimodal distribution with azimuths which dip to the northeast and southwest (Fig. 5).

5.1.2. Lithofacies Association 2 (LFA N2; interbedded diamicton, gravel, sand and mud)

LFA N2 consists of gently-dipping to horizontal beds of brown (7.5YR 5/4), matrix-supported diamicton (stratified, laminated and massive), granule gravel (GRfu, GRm), sand (Suf, Sr, Sh, Sd, Sm, Sl) and mud (Fd(d), Fd). Although the diamicton facies are not graded

Table 2
Classification of lithofacies and lithofacies associations (LFA) at Noer, Stohl and Altbülk.

Site	LFA	Component facies and facies codes	Description	Interpretation
Noer	LFA1	Massive diamicton (Dmm)	Massive, matrix-supported diamicton that is clast poor and fissile in appearance.	Deposition as a subglacial till.
	LFA2	Stratified and laminated diamicton (Dms/Dml); upward fining and massive granule gravel (GRfu/GRm); upward fining, rippled, horizontally bedded, deformed, massive and laminated sand (Suf/Sr/Sh/Sd/Sm/Sl); and deformed silts and clays (Fd) with dropstones (Fd(d))	2–3 m massive, matrix-supported diamicton intercalated with sorted gravels, sands and muds giving it a bedded appearance. Outsized clasts occur throughout the sorted sediments. Thickness of beds varies from a few mm to ~1 m and contacts are conformable. The base of the LFA has been deformed, with convolute beddings, flame structures and sheared and loaded boundaries.	Deposition in a glaciolacustrine environment by a combination of rain-out, current reworking and flow remobilization.
	LFA3	Deformed laminated to stratified diamiction (Dml/Dms); chalk, sand (Sd); and mud (Fd) with outsized clasts (Fd(d)/Sd(d))	Intensely deformed 1–2 m mélange of stratified diamicton, chalk, sand and mud. Outsized clasts occur and have downwarped and are draped by bedding. Beds dip towards the SW.	Glaciotectonised or debris flow unit.
	LFA4	Stratified to massive diamicton (Dms –> Dmm); and deformed sand rafts (Sd)	>5 m massive, matrix-supported diamicton that is clast poor, and fissile in appearance. Bedding structure in lower portion of unit imparted by horizontal to sub-horizontal chalk stringers. Rafts of sand that have been deformed and sheared nested within diamicton.	Deposition as a subglacial till.
Stohl	LFA1	Stratified to laminated diamicton (Dms/Dml); deformed sand (Sd); and mud (Fd) partings	8–10 m of stratified and laminated diamicton. Bedding imparted by mm- to cm- thick partings of sand and mud, and by beds of clay-rich and silt-rich diamicton. Clasts are rare within the diamicton. Large (m-scale) folds, augen structures and competent masses of sand and diamicton observed towards base of LFA.	Deposition in a glaciolacustrine environment by a combination of rain-out, current reworking and flow remobilization. The base of the LFA has been glaciotectonised.
	LFA2	Upwards fining and clast-supported, imbricated (a(p)a(i)) gravel (Gfu/Gmi); horizontally stratified and upward fining granule gravel (GRh/GRfu); massive and horizontally stratified sand (Sm/Sh); and thin interbeds of diamicton (Dmm)	Shallow (0.5–1 m), 1–10 m wide channel fills. Clast-supported, locally imbricated granule and pebble gravel that coarsens towards centre and base of trough. Upwards fining into granule gravel and coarse sand. Crude stratification at top of fill imposed by openwork granule gravel, bedded sand and thin diamicton interbeds.	Deposition from high concentration channelized density flows.
Altbülk	LFA1	Stratified diamicton (Dms); and stringers of bedded sand (Sl)	0.5 m thick stratified, matrix supported diamicton. Stratification imparted by mm-thick horizontally bedded sand stringers.	Deposition in a proglacial glaciolacustrine environment dominated by suspension settling and current reworking.
	LFA2	Massive gravel (Gm); deformed, rippled, laminated and horizontally bedded sand (Sd/Scr/Sl/Sh); laminated and massive silts and clays (Fl/Fm); and matrix supported, stratified diamicton (Dms)	~4.5 m unit dominated by laminated clay and silt, climbing ripples and horizontally bedded sand. Interbed of clast-poor, matrix-supported diamicton with sag and flame structures and a sheared lower contact and loaded upper contact.	Deposition in a proximal to distal glaciolacustrine environment by a combination of bottom current transport, suspended sediment settling and debris flows.
	LFA3	Stratified to massive diamicton (Dms –> Dmm); and horizontally bedded, laminated and deformed sand (Sh/Sl/Sd)	<1 m of matrix supported diamicton. Basal 0.5 m stratified due to presence of horizontally bedded sand. The diamicton becomes more massive upwards.	Deposition either as a subglacial till or debris flow.

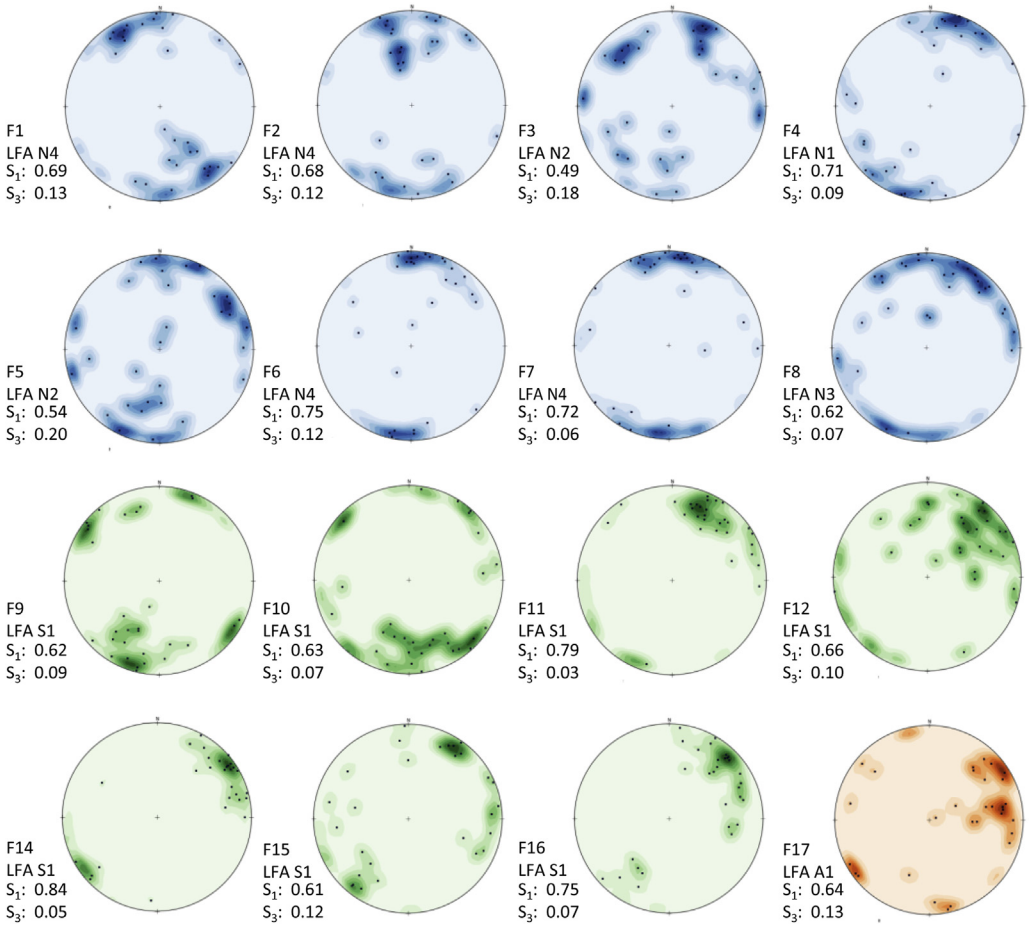

Fig. 5. Clast fabric data collected from diamictons at Noer (blue), Stohl (green) and Altbülk (red) plotted using OpenStereo with (equal area) hemispheric projection and contoured using the natural neighbour method. See stratigraphic logs for locations. (For interpretation of the references to colour in this figure legend, the reader is referred to the web version of this article.)

internally, the intercalated sediments are often distinctly bedded, with horizontal laminations, upward-fining successions and current ripple structures evident (Figs. 6a,b). The thickness of the individual lithofacies varies from a few mm to ~1 m, giving the whole 2–3 m thick LFA a stratified appearance. Where the sand is current bedded, ripples reveal a palaeo-current direction towards the east. In logs 3 and 4 the rippled surface is conformably overlain by diamicton, which delicately drapes the undulating surface below (Fig. 6b). Packages of upward-fining granule-gravel, sand and occasionally laminated clay/silt occur repeatedly between diamicton layers and can in places be traced tens of metres along the cliff. Occasionally, these packages are associated with concave, erosional lower contacts that pinch out laterally over several decimetres (Fig. 6c). Outsized clasts and infrequent pods of coarse sand and gravel occur throughout the sorted sediments, either penetrating or bending the substratum.

The base of LFA N2 consists of a discontinuous mélange of contorted, clast poor, clay-rich diamicton, sand and clay with convolute bedding, flame structures, small intra-clasts of underlying material associated with sheared (rip-up clasts) and loaded boundaries, disrupted pods and lenses and sub-horizontal silt/sand stringers. Primary sedimentary structures are only partially preserved, and the facies tend to pinch and swell laterally. Further evidence of deformation is provided by eastward-curving sediment lenses (Fig. 6d), which rise through the diamicton mélange and are composed of massive to stratified sand, with rare dropstones, and pods of silt, granule-gravel and diamicton. These features, which are ~70 cm tall and reach up to 25 cm wide at their base bend round larger clasts in the diamicton and both taper and splay upwards. Fold structures include the identification of parasitic folding of intercalated diamicton, sand and clay around a more competent mass of protruding diamicton. Localised, centimetre to decimetre scale reverse and normal faulting is also recorded, particularly where the primary sedimentary structure has been partially preserved, such as in the warped and faulted stratified sand and granule-gravel facies at the base of log 5.

Two fabrics were taken in LFA N2, one in the lower mélange (F3) and another in the upper less-deformed succession (F5) (Fig. 5). Both show multimodal clustering with weak S_1 values of 0.49 (F3, log 1) and 0.54 (F5, log 4). A predominance of NW/N dipping clasts is noted in F3, which matches the local dip of the palaeo-surface, and both fabrics contain relatively steeply dipping clasts.

5.1.3. Lithofacies Association 3 (LFA N3; deformed diamicton, sand and mud)

Above LFA N2, at the eastern end of the exposure (logs 5 and 6), is an intensely deformed 1–2 m thick mélange of laminated to stratified diamicton, chalk, sand and mud (LFA N3) (Fig. 6e,f). Diamicton balls and flame structures are common as are clay, silt and sand pods/stringers and pockets of granule to pebble gravel. Outsized clasts (up to 40 cm) within the diamicton mélange have downwarped or penetrated underlying laminae and are in turn

draped by overlying strata. Where underlying lamina has been disturbed by larger stones small, longitudinally asymmetrical folds form below the clasts, indicating lateral drag towards the east and south (Fig. 6e). In log 6 the entire succession dips up to 22° towards the SW/W. A fabric taken from the centre of LFA N3 in log 5 (F8) had a moderate ($S_1 = 0.62$), spread-unimodal distribution and a mean lineation azimuth which dips towards the NNE (Fig. 5).

A thin section taken near the base of LFA N3 (TS-D) reveals a lower massive diamicton with sub-vertical fissures (Fig. 7). This leads up into a sub-horizontal sand lamina, with an erosional, undulating to stepped lower boundary and convolute transition into a capping silt facies. Diamicton pellets, outsized clasts and minor ductile deformation structures are evident within this zone. The diamicton above the lamina has a distinctive sub-horizontal structure imparted by numerous undulating laminations of (normal and inverse) graded sand/silt, clay-rich and -poor diamicton and horizontally aligned clasts. Laminae are warped below and above larger clasts, which are themselves often plastered with clay. Rotation structures are common and there is a weakly-developed skelsepic plasmic fabric.

5.1.4. Lithofacies Association 4 (LFA N4; partially bedded matrix-supported diamicton)

LFA N4 is a brown (7.5YR 5/4) to dark grey (7.5YR 4/1) matrix-supported diamicton that has a bedded appearance imparted by cm-thick chalk stringers that become less frequent towards the top of the >5 m thick LFA. The chalk stringers are horizontally to sub-horizontally aligned, undulating to anastomosing, and downwarp below or are penetrated by larger pebbles. In the lowermost 20 cm pods and stringers of sand and chalk have been partially deformed. At log 5, at the boundary with LFA N3, this has resulted in a kinked fold structure and associated reverse faults indicating NE–SW compression (Fig. 8f). The boundary with LFA N2/3 varies from gradational at logs 5 and 6 to loaded and sheared at log 1. Two large (~0.5 m) deformed sand rafts with granule to pebble gravel and pockets of diamicton float within LFA N4 at the eastern end of the exposure (log 1). The boundary between the rafts and the surrounding Dmm is sheared and convoluted. Four fabrics were recorded in LFA N4 (F1, 2, 6, 7) spaced laterally across the exposure (Fig. 5). All display moderately-strong clustering, with S_1 values that range from 0.68 to 0.75 and plot as spread unimodal with azimuths which dip to the NW–SE (F1) and N–S (F2, 6, 7).

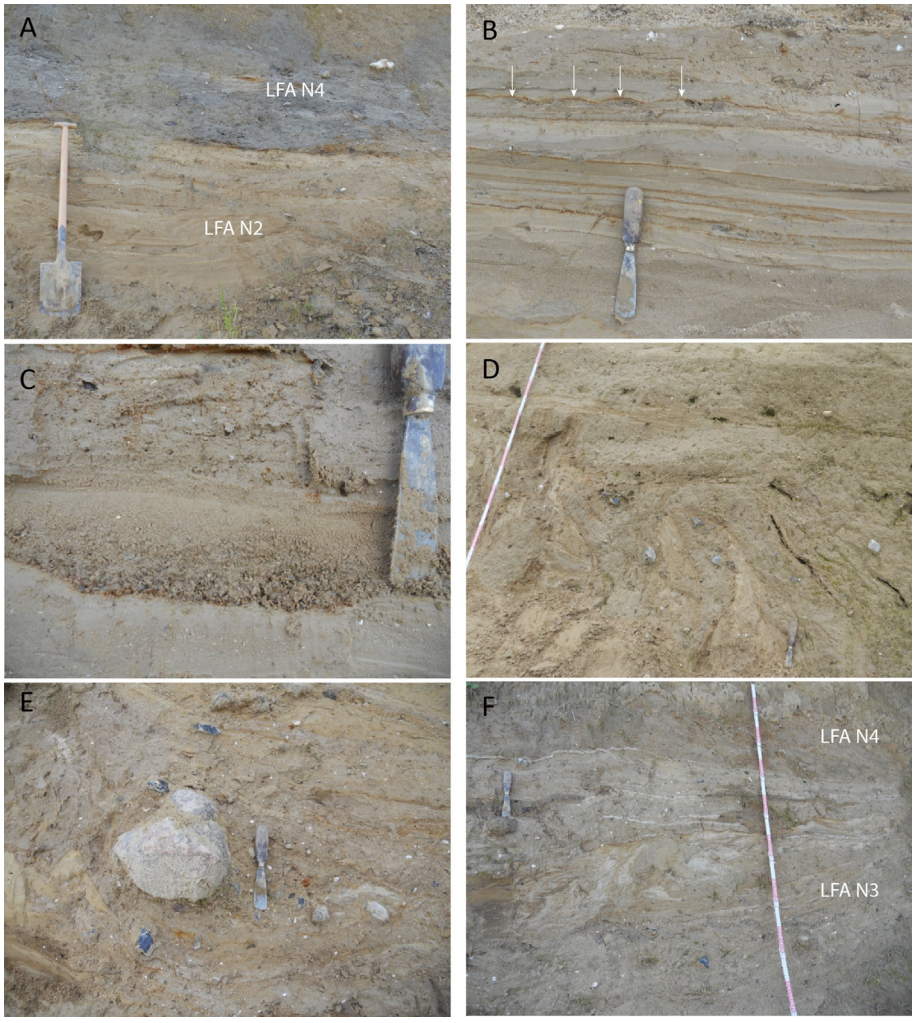

Fig. 6. Photographs of lithofacies exposed at Noer. A: Horizontal beds of diamicton, sand and mud, partially deformed in the central bottom portion of the picture (LFA N2), overlain by a grey diamicton (LFA N4) containing cm-thick chalk stringers that become less frequent towards the top. B: Close up of LFA N2 illustrating the ripple structures (arrowed) conformably overlain by diamicton. C: Example of a small scour-and-fill structure that fines upwards and is conformably overlain by diamicton. D: Eastwards curving sediment lenses (~70 cm tall) that rise through the diamicton mélange. E: Outsized clast within the diamicton mélange of LFA N3. Note the small asymmetric fold to the east (left) of the clast and the concentration of clasts in its lee-side (right). F: Intensely deformed 1–2 m thick mélange of laminated to bedded diamicton, chalk, sand and mud (LFA N3). Note that deformation is concentrated towards the centre of the image, and that the transition into LFA N4 is marked by kinked bands.

5.1.5. Grain size analysis

Grain size analysis reveals that the diamicton matrices at Noer are equivalent, with about 10% clay, 40% silt and 50% sand (Fig. 8). LFA N4 is slightly more silty and contains less sand. The lithological components also show little variability and exhibit spectra typical for diamictons deposited by ice of north-easterly provenance (e.g. Piotrowski, 1994; Kjaer et al., 2003). This includes a high proportion of far-travelled components, including Palaeozoic limestone (20–40%) sourced from the Baltic and crystalline rocks (60–70%) from the Fennoscandian Shield (Fig. 8).

5.2. Stohl

We investigated exposed glacigenic sediments along 360 m of the east-west orientated, 10–16 m high Baltic Sea cliff near Stohl (54°28.753′ N, 10°08.781′ W). Five sedimentary logs were recorded along the length of the exposure (Fig. 9). Stratified and laminated diamicton is exposed throughout the succession (8–10 m thick), along the entire length of the cliff (Table 2). Typically sub-horizontally bedded, the diamicton undulates and anastomoses around structures such as folds, rafts and channel-fills. The base of the succession had slumped considerably making it difficult to observe the transition into the lower facies (U1), which has been interpreted both as a lodgement (Piotrowski, 1992) and deformation till (Hart et al., 1996, although see reply by; Piotrowski et al., 1997).

5.2.1. Lithofacies Association 1 (LFA S1; Stratified and laminated diamicton)

LFA S1 is composed of stratified and laminated diamicton and is observed throughout the succession. It corresponds to facies U2 of Piotrowski (1992), which was interpreted as a melt-out till.

Log 1 was recorded at the western end of the investigated exposure at ~8 m a.s.l. (Fig. 9). It comprises 2 m of grey (7.5YR 5/1) to brown (7.5YR 5/3), stratified to laminated matrix-supported diamicton. The bedding is imparted by mm-to cm-thick partings of sand and mud (Sl, Sd, Fm) that occur every 1–2 cm in places (Fig. 10c). Clasts within the diamicton are rare and predominantly

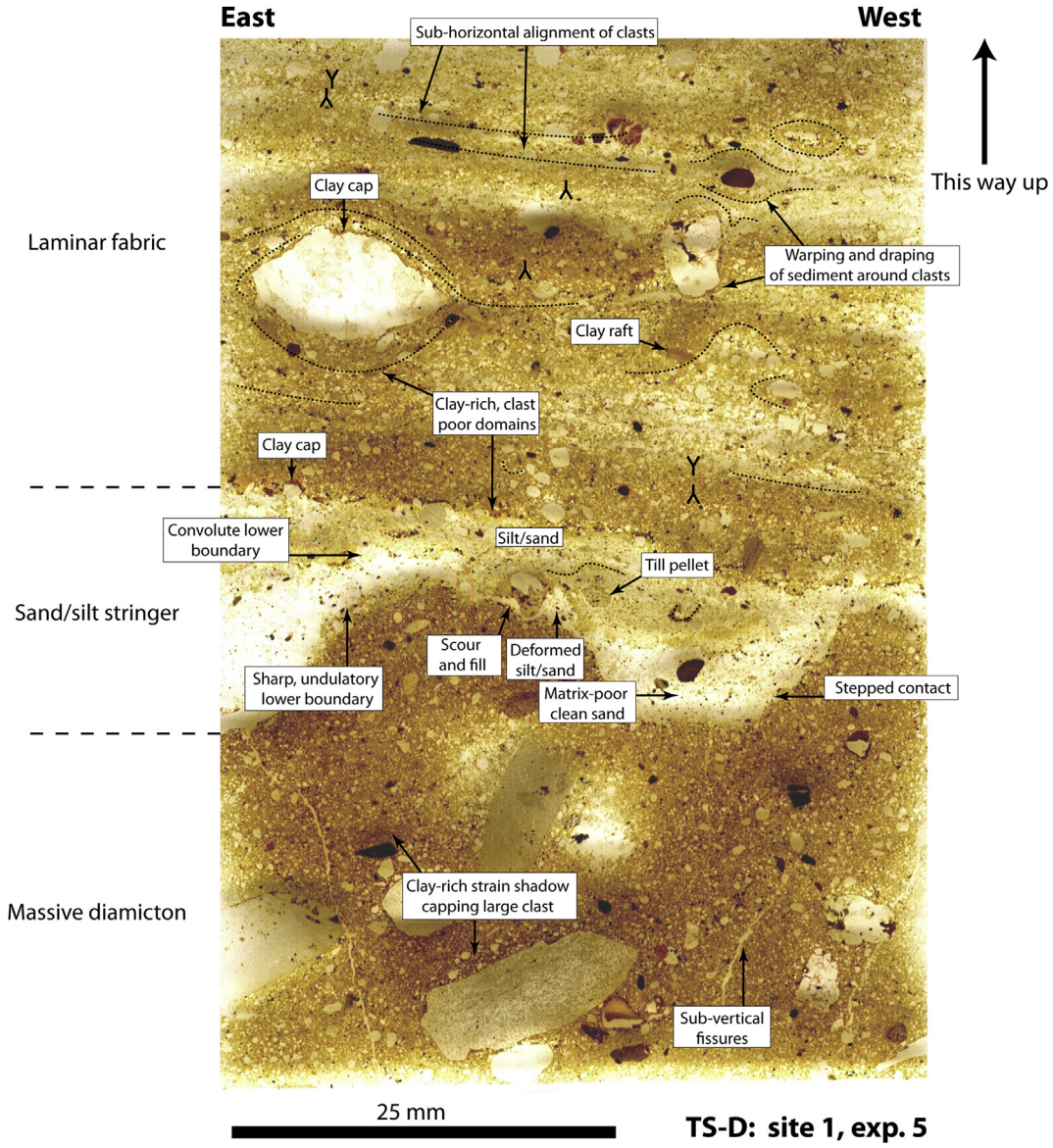

Fig. 7. Annotated scan of sample TS-D from Noer. This thin section is taken near the base of the diamicton mélange of LFA N3 at log 5 (see Fig. 4). Note the scoured sand fill and the upper sub-horizontally bedded diamicton.

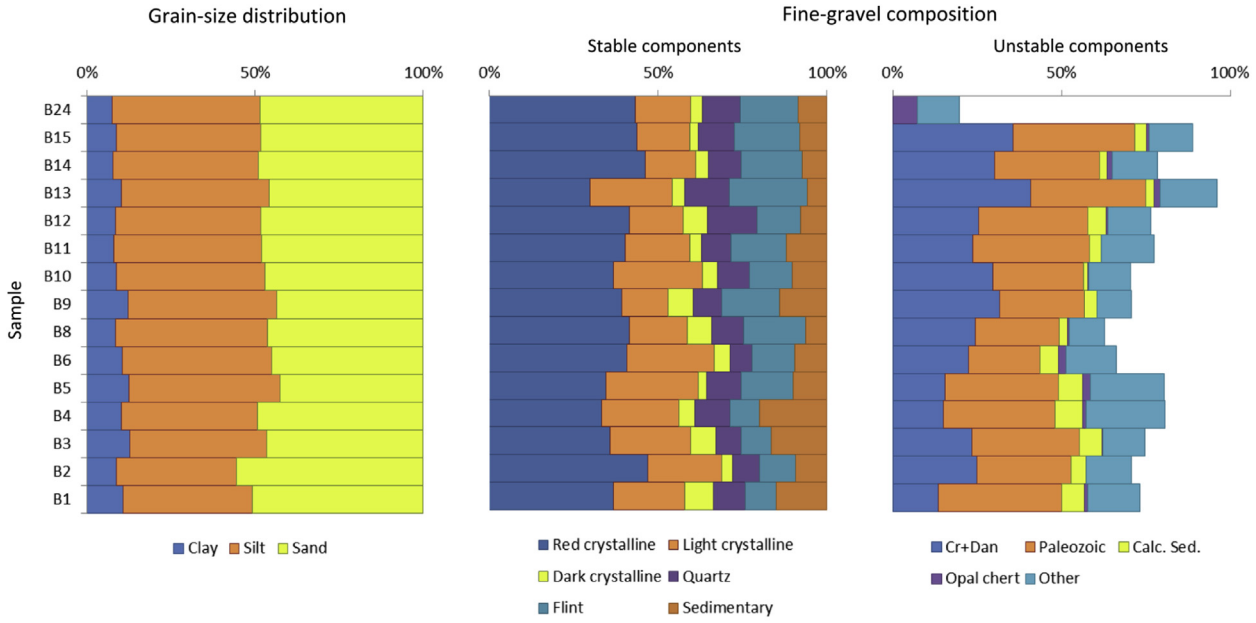

Fig. 8. Grain size distribution (fraction ≤ 2 mm) and fine gravel lithology for Noer, Stohl and Altbülk. Lithological composition was determined on a minimum of 300 grains in the 2–4 mm size fraction. Red, Light and Dark refer to coloured crystalline components. Cr + Dn = Cretaceous and Danian chalk; Paleozoic = Paleozoic limestone; Calc. Sed. = calcareous sedimentary rocks. The counting results are presented separately for stable and unstable lithologies whereby the sum of stable components gives 100% to enable sample-to-sample comparison not biased by weathering. (For interpretation of the references to colour in this figure legend, the reader is referred to the web version of this article.)

granule-gravel sized, with some pebbles. Beds dip up to 32° towards the S and SW. Lower in the succession the bedded appearance is imparted by mm-thick, darker-coloured diamicton lamina that become less frequent down-exposure. A thin section taken across one of the darker lamina shows clast-poor, clay-rich domains up to 10 mm thick, characterised by sharp, undulating upper contacts and conformable to graded lower contacts (Fig. 11). Small (mm-offsets), steeply-dipping normal faults cut through the domains.

The bedded succession is punctuated by a SW-dipping recumbent fold (Fig. 10e). A large (10 cm) clast towards the base of the structure penetrates a sand stringer and is draped by overlying facies. Laterally discontinuous, regularly spaced, mud and sand stringers pervade the upper half of the exposure (Fig. 10c). A thin section taken through the diamicton reveals an interbedded succession of stratified clay- and sand-rich diamicton and laminated normally-graded diamicton, sand and mud (Fig. 12). The laminae drape and are downwarped beneath clay-coated clasts. Two clast fabrics (F9, F10) show moderately strong clustering, with S_1 values of 0.62 and 0.61 (Fig. 5). Both plot as spread bimodal distributions showing NW–SE and NNE–SSW dipping clasts, although the majority dip SE to SSW.

Logs 2a,b are composed of a 5 m grey (7.5YR 5/1), stratified, matrix-supported diamicton (Dms). Stratification is imparted by the presence of pale and dark diamicton domains (Fig. 10b) and mm-to cm-thick sand partings equivalent in character to log 1 (Fig. 10a,f). Clasts have downwarped the underlying substratum and are draped by overlying facies. Laterally continuous sand stringers tend to occur as clusters, while discontinuous stringers and deformed pods of sand occur infrequently throughout. Beds dip up to 32° towards the N and NE. Two fabrics (F11, F12) were measured in the diamicton at log 2a (Fig. 5). F11 shows strong unimodal clustering (S_1 value of 0.79), while F12 shows a spread unimodal distribution, steeply dipping clasts and a moderately-strong S_1 value of 0.63. In both fabrics clasts tend to dip towards the NE.

Log 3 is a 3 m exposure just to the east of log 2b, the bottom 2 m of which overlaps, although the sand partings (some of which show internal bedding) become more densely spaced (occurring every 3–6 cm). Two fabrics (F14, F15) record NE dipping azimuths with F14 displaying strong unimodal clustering (S_1 = 0.84) and F15 spread unimodal clustering (S_1 = 0.61) (Fig. 5).

Log 4 was recorded towards the top of the exposure and consists of a largely massive, grey (7.5YR 5/1), matrix-supported diamicton. Some stratification is imparted by mm-thick lamina of paler diamicton and internally-bedded sand partings up to a few-cm thick. A fabric (F16) taken at the top of the section records moderately strong (S_1 = 0.75), unimodal clustering and azimuths that typically dip towards the NE (Fig. 5).

Large (metre-scale) amplitude folds, augen structures, deformed rafts of sand and competent masses of diamicton are observed towards the base of LFA S1, which are in-turn draped by stratified and laminated diamicton (Figs. 9 and 10d,h). In some cases it is clear that these structures sit within the diamicton in which case the bedding seem to diverge around them, whereas in others they may underlie it. The most impressive example is of a >5 m high upright fold with hooked limb (Fig. 10d) indicating compression during NW flow. Large (several metres in diameter), deformed sand rafts and augens nested within the stratified/laminated diamicton show evidence of folding, rotation (tails) and shearing. In one example stratified diamicton underlying a large sand raft had been deformed producing an isoclinal recumbent fold structure.

5.2.2. Lithofacies Association 2 (LFA S2; Massive to diffusively graded-stratified gravel and sand)

Nested within LFA S1 are a number of shallow (0.5–1 m), 1–10 m wide channel-fills (LFA S2) (Figs. 9 and 10g). At log 3, LFA S2 pinches out laterally over a distance of ~10 m and is composed of massive to diffusively graded-stratified gravel (Gfu, Gmi, GRh, GRfu), sand (Sh, Sm) and pods of soft diamicton (Table 2). Clast-supported granule and pebble gravel coarsens towards the centre and base of the trough and fines upwards into clast-to matrix-supported granule

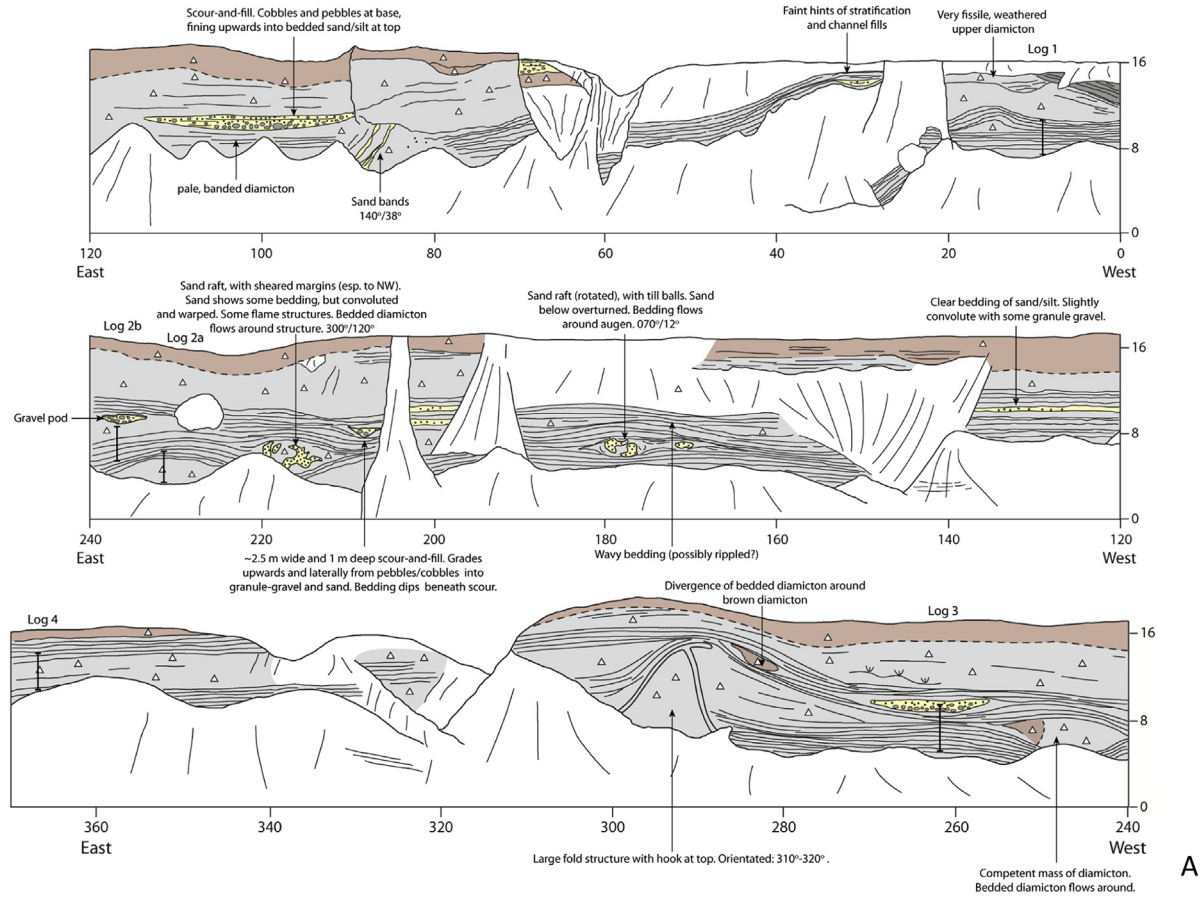

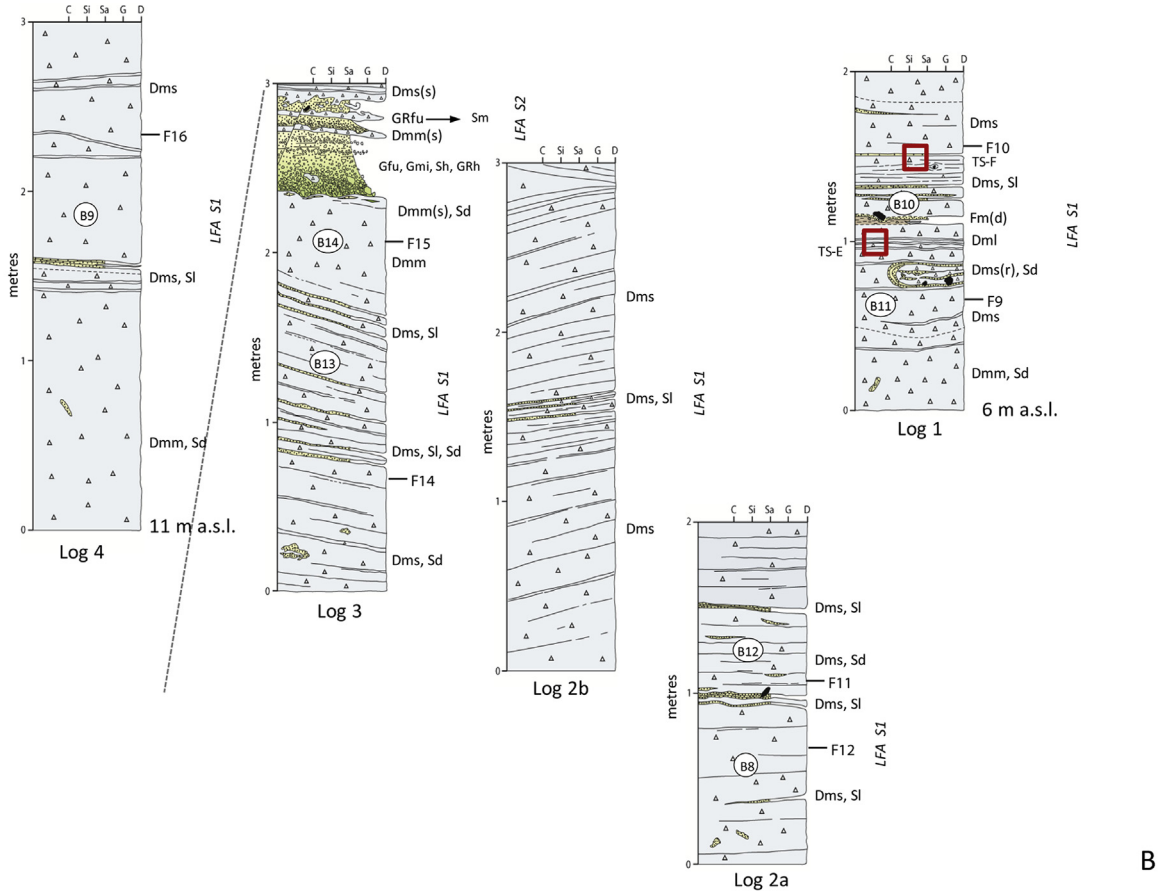

Fig. 9. Stratigraphic logs at Stohl. White areas in the section log (A) were not exposed. The location of thins sections (TS), bulk samples for clast lithology and particle size (B) and fabrics (F) are illustrated on the vertical logs. Lithofacies codes are based upon those of Evans and Benn (2004) (see Table 2 for classification of lithofacies and lithofacies associations).

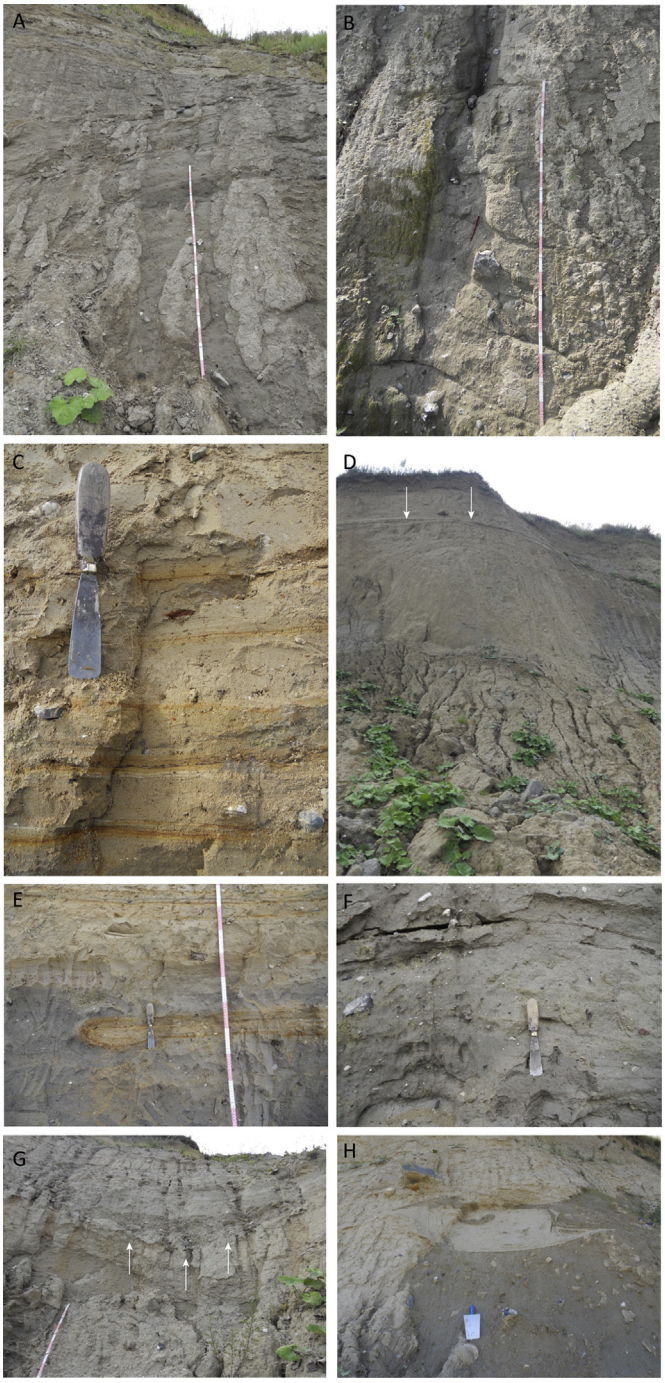

Fig. 10. Photographs of lithofacies exposed at Stohl. A: Sub-horizontally bedded, stratified and laminated diamicton. B: Example of paler and darker bands within LFA S1, which produces a bedded appearance (see Fig. 11 for thin section that cuts across the banding). C: Diamicton interbedded with mm-to cm-thick partings of sand and mud (see Fig. 12 for thin section displaying the finely laminated structure of these partings). D: >5 m high upright fold of waterlain sediments with hooked limb indicating NW flow. Note that further waterlain sediments (arrowed) drape the top of the fold. E: Recumbent fold of diamicton, sand and mud. Note that above and below the fold the sediments are horizontally bedded. F: Diamicton with partings of mm-to cm-thick partings of sand and mud that have been partially washed out towards top of image. G: Small (~1 m) channel fill (base arrowed) composed of bedded gravel (LFA S2). Note that the channel fill is formed in a syncline of bedded diamicton. H: Sand augen with tails indicating rotation during eastwards flow.

gravel and coarse sand. Crude stratification towards the top of the channel fill is imposed by thin beds of openwork granule-gravel, horizontally-bedded sand, and thin diamicton interbeds characterised by abrupt lower contacts and loaded upper contacts. The coarse gravel facies at the base is imbricated (a(p)a(i) fabric), with measurements indicating a flow direction towards the SW.

5.2.3. Grain size analysis

The results of the grain size analysis are remarkably consistent throughout the succession comprising ~10% clay, 45% silt and 45% sand (Fig. 8). The top-most diamicton (from log 4) is slightly finer-grained, with a higher percentage of clay relative to sand. The analysis is comparable to Noer, although there is a higher fraction of silt. The distribution of fine-gravel components is fairly uniform across all seven samples, possibly apart from sample B13 which has somewhat less red crystalline rocks, more chert and more Cretaceous and Danian chalk. However, these differences are within a typical range of variations characterizing one and the same diamicton unit derived from ice advance of NE provenance, similar to the Noer site.

5.3. Altbülk

At Altbülk (54°27.898′ N, 10°10.578′ W) we focused on a 6 m high vertical section (Fig. 13). In contrast to Noer and Stohl the bulk of the succession comprises sorted sand and mud, sandwiched between two diamictons (Table 2).

5.3.1. Lithofacies Association 1 (LFA A1; diamicton)

At the base of the Section 0.5 m of brown (10YR 5/3) matrix-supported diamicton was recorded (LFA A1) (Fig. 14a). It has a stratified appearance imparted by mm-thick, horizontally-bedded sand stringers, which undulate, pinch out and are downwarped beneath larger clasts. Fabric F17 records a spread-bimodal distribution, with moderate clustering (S_1 value of 0.64), and clast azimuths which predominantly dip towards the NE (Fig. 5).

5.3.2. Lithofacies Association 2 (LFA A2; sorted gravel, sand and mud interbedded with diamicton)

The bulk of the sedimentary succession (~4.5 m), LFA A2, consists of sorted gravel, sand and mud (facies: Gm, Sd, Scr, Sl, Sh, Fl, Fm) with a thin (~30 cm) inter-bed of clast-poor, loaded diamicton (Dms). The basal 2 m of LFA A2 fines upwards through ~10 cm of clast-supported, granule- and pebble-gravel into massive to rippled sand, and laminated mud. The gravel facies pinches out laterally, has an erosional lower contact, and is draped by a thin mm-thick silt layer (Fig. 14a). One of the pebbles appears to have sunk into the underlying Dms. This facies is overlain by massive sand with rare granule gravel that in turn grades into type-A climbing ripples (Jopling and Walker, 1968) recording a NW palaeo-current direction (Fig. 14b). A series of normal faults with ~1 cm offsets show displacement towards the south. Conformably draped over the climbing ripples is a clay bed overlain by ~2 m of wavy, sub-cm laminations (Fig. 14c). Micromorphological analysis of the laminations (Fig. 15) shows alternations of silt (coarse component) and clay (fine component) laminae that are identified as a couplet (see Palmer et al., 2008; Livingstone et al., 2010). The coarse component grades into the fine component (clay) and consists of silt with some fine sand in places. The fine component has a sharp upper contact. Couplets vary from <1 mm up to 1 cm thick and the coarse component is typically about twice the thickness of the fine component. The laminae have been faulted by a series of shallow-angled reverse faults at the base of the succession and steeply dipping normal faults further up. The clay at the base of the thin

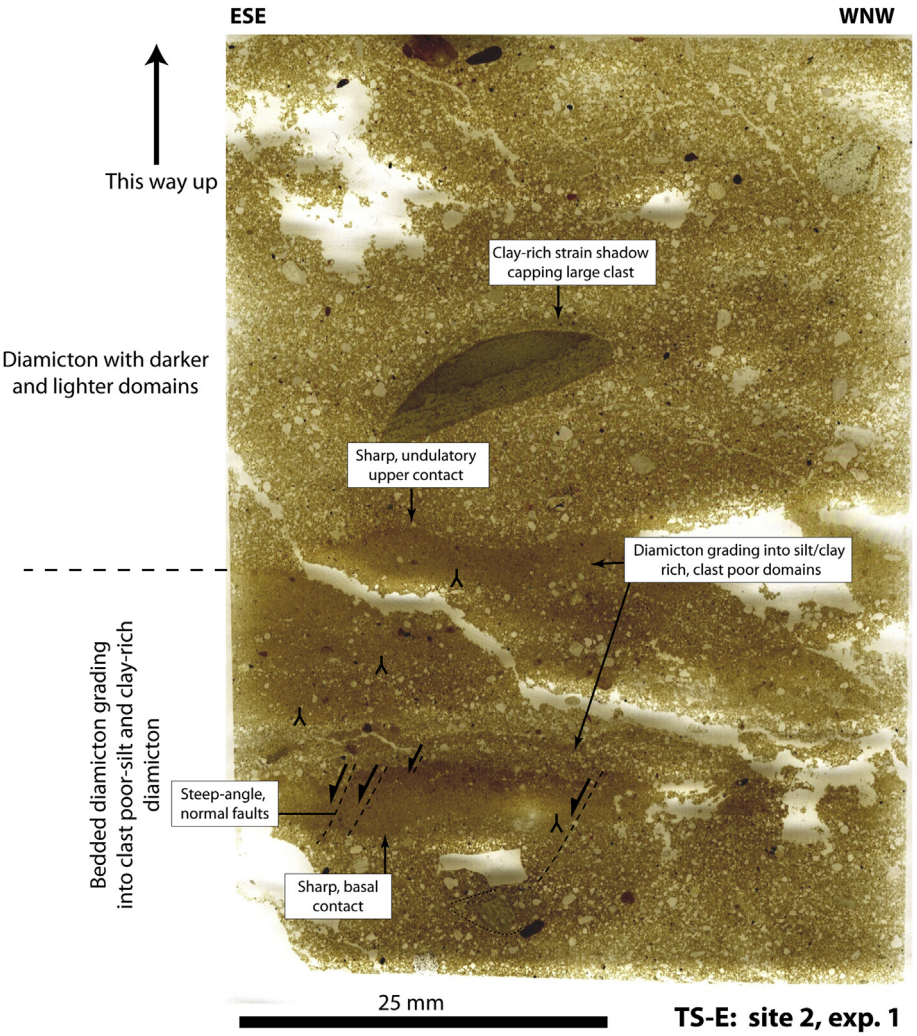

Fig. 11. Annotated scan of sample TS-E from Stohl. This thin section is taken across one of the darker bands in the bedded diamicton of LFA S1 at log 1. The darker band correlates to the clay-rich domains that are characterised by graded lower and sharp upper contacts.

section is heavily contorted, displaying flame and water-escape structures.

Laminated silt–clay couplets are interrupted by a thin, brown (10YR 5/3), matrix-supported diamicton almost devoid of clasts (Fig. 14d). It has a sheared lower contact, and loaded upper contact characterised by sag and flame structures that has resulted in a contorted admixture of diamicton and silt.

Micropalaeontological investigation of three bulk samples taken from the laminated silt–clay facies (B17, 19 & 22, Fig. 13) at Altbülk revealed single specimens of foraminifer *E. excavatum* and single Cretaceous foraminifers in B17 only. Although well preserved, given its very low abundance *E. excavatum* is most likely re-worked, probably from marine Quaternary deposits on Rügen, NE Germany (e.g. Wiegank, 1972; Steinich, 1992).

5.3.3. Lithofacies Association 3 (LFA A3; diamicton with gravel, sand and silt interbeds)

The upper 3 m of the exposure coarsens from clay–silt laminations via silt-sand laminations and horizontally-bedded sand into a thin (<1 m thick) capping diamicton (LFA A3) (Fig. 14e). LFA A3 is a weathered, brown matrix-supported diamicton. In the lower 0.5 m it comprises a stratified diamicton, defined by the presence of horizontally interbedded granule-gravel, sand and silt. The beds of sand increase in thickness into LFA A2 below. This Dms grades upwards into a more massive diamicton (Dmm).

5.3.4. Grain size analysis

Grain size analyses of the lower and upper diamicts are comparable to sites 1 and 2, with about 10% clay, 40% silt and 50% sand (Fig. 8). In contrast, the thin brown diamicton in the centre of the succession contains a higher fraction (~60%) of silt. Stable lithological components of the two diamicton samples taken at the bottom and at the top of the succession are nearly identical. However, the top sample (B24) has a depleted content of unstable components, indicating that it has been weathered. Apart from the impact of weathering, these diamictons closely resemble those at Noer and Stohl.

6. Interpretation of glacigenic deposits

6.1. Deposition in a glaciolacustrine environment proximal to or beneath an ice mass (LFA N2-3, S1-2, A1)

The co-existence of diamicton conformably intercalated with sorted gravel, sand and mud (LFA N2-3, S1-2, A1) suggests contemporaneous deposition in a glaciolacustrine environment

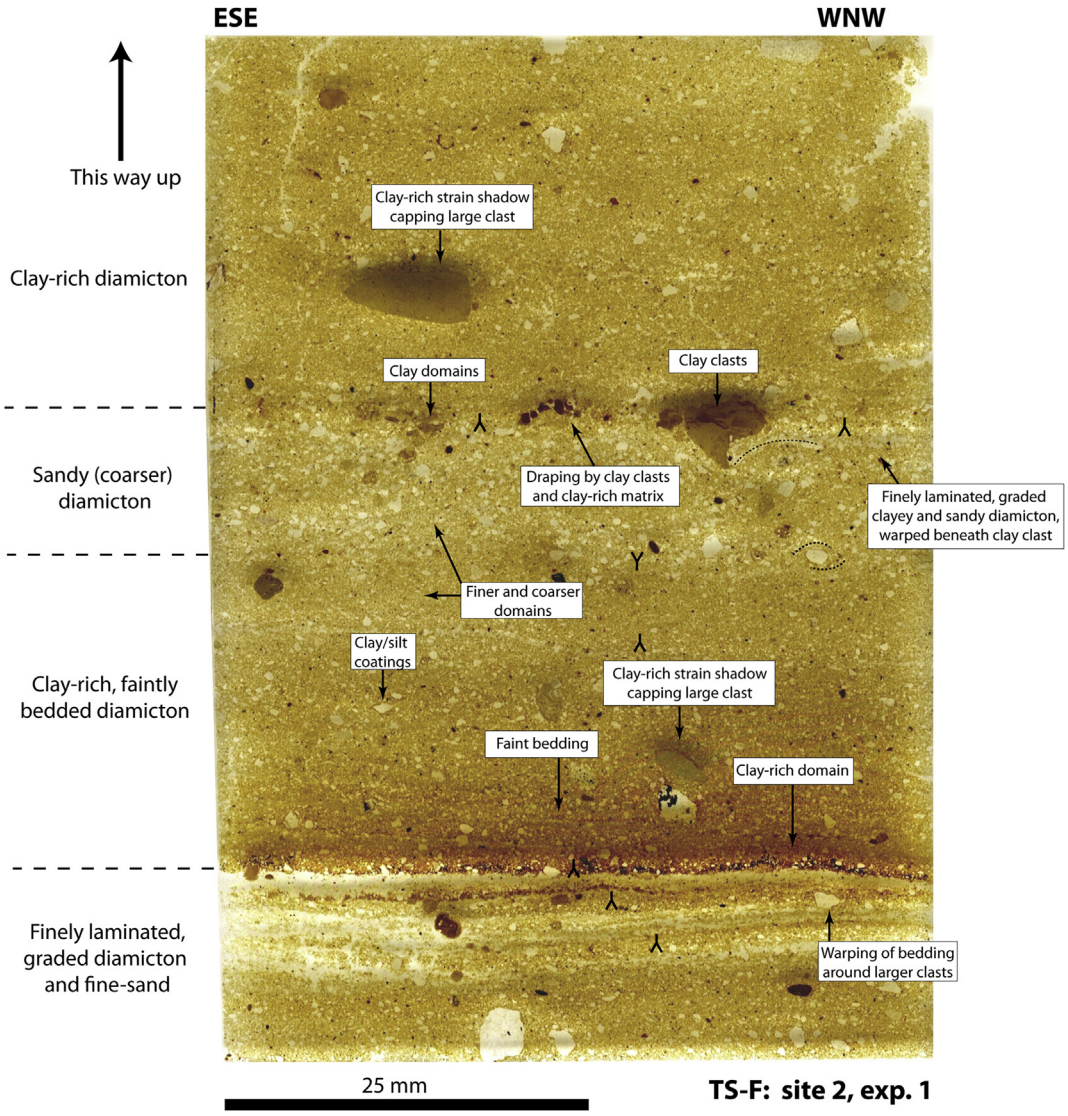

Fig. 12. Annotated scan of sample TS-F from Stohl. This thin section is taken across diamicton interbedded with sands and muds at log 1. Note the finely laminated structure and gradational contacts.

proximal to or beneath an ice mass by a combination of rain-out, current reworking and flow remobilization (e.g. Evenson et al., 1977; Gibbard, 1980; Eyles, 1987; Eyles et al., 1989; Bennett et al., 2006; Lee and Phillips, 2008; Ravier et al., 2014a). This agrees with previous work by Piotrowski (1994a), although we extend the interpretation to include 'melt-out' tills of his upper complex (Piotrowski, 1992, 1996).

The widespread occurrence of dropstone and dump structures in all associated LFAs demonstrates melt-out of debris from sediment-laden icebergs and/or an ice ceiling. This includes penetration, bending, rupture and rucking of the underlying substratum, and fold-structures and pressure shadows from remobilization (Thomas, 1984; Thomas and Connell, 1985). Individual units of diamicton conformably separated by waterlain facies (e.g. LFA N2, Fig. 6) represent discrete sediment-density flows (Evenson, 1977; Eyles et al., 1987) and pulses of debris raining out from an ice-roof (Gibbard, 1980; Bennett et al., 2006). Subaqueous sedimentation of diamicton through a water column by low-energy rain-out is best illustrated at LFA N2 where underlying ripple structures have been preserved and are conformably overlain by diamicton (Fig. 6b) (Piotrowski, 1994a).

Beds showing current ripple structures (Sr, LFA N2), openwork granule gravel (GRh, LFA S2) and laminated sand and mud (Sh, Sl, Fl, Fm, all LFAs) (Table 2) indicate punctuated sedimentation by bottom current transport and suspended sediment settling (e.g. Jopling and Walker, 1968). Decimetre-scale scours infilled with normally-graded sand (LFA N2, Fig. 6c), are interpreted as the product of rapid cut-and-fill processes associated with jet flows that underwent a hydraulic jump (Winsemann et al., 2007, 2009). These cut-and-fill structures are typically associated with subaqueous ice-contact fan deposits (e.g. Russell and Arnott, 2003; Winsemann et al., 2009).

At Noer and Stohl (LFA N2-N3, S1-2) the principle mode of sedimentation was remobilization by cohesive and cohesionless density flows. Micro-laminae of normally graded clay-rich, clast-poor diamicton (dark beds), separated by massive diamicton (LFA S1, Fig. 11), suggest repeated subaqueous sedimentation by hyperconcentrated sediment-density flows capable of inhibiting sorting in all but the dilute mixing cloud at the top of the boundary layer (Eyles, 1987; Mulder and Alexander, 2001; Bennett et al., 2002). These types of flows often occur close to the grounding-line where channels debouch into lake water (Plink-Björklund and Ronnert,

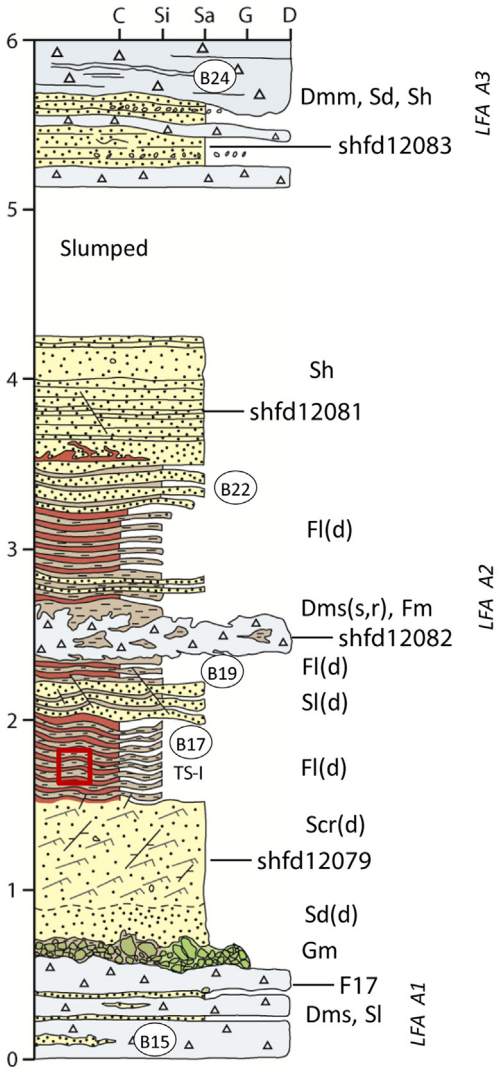

Fig. 13. Stratigraphic log at Altbülk. The location of thins sections (TS), bulk samples for clast lithology and particle size (B), OSL samples (shfd code) and fabrics (F) are illustrated on the vertical log. Lithofacies codes are based upon those of Evans and Benn (2004) (see Table 2 for classification of lithofacies and lithofacies associations).

1999). Laminae of graded silty-sand finely interbedded with diamicton (LFA S1, Figs. 10c and 12) are interpreted as being deposited by the rapid rain-out of sediment-laded underflows or as thin-bedded turbidites (Gravenor et al., 1984; Eyles et al., 1989; Lee and Phillips, 2008). Alternatively the laminae may reflect winnowing of clay and silt facies by currents in an environment dominated by rain-out (Eyles et al., 1989; McCabe & Ó Cofaigh, 1994; Wysota, 2007). In LFA S1 (Fig. 12), rip-up clasts of laminated clay and crude sorting of the thicker intrabeds of matrix-rich diamicton are consistent with a density-flow origin, while dropstones attest to ice-rafted melt-out. Thick successions of stratified/laminated diamicton, sand and mud (all LFAs, Table 2) reflect pulses of diamicton being introduced into a standing water body.

LFA N3 comprises undulating, sub-horizontal stringers of chalk, sand and mud (e.g. LFA N3, Fig. 6f) that have been heavily contorted and fluidized, creating a distinctive streaky appearance typical of wet-type debris flows (Gravenor et al., 1984; Lachniet et al., 1999, 2001; Roberts and Hart, 2005). Variably sorted diamicton, sand and mud that bend around larger clasts; the preferential alignment of coarse sand and fine gravel with their long axes parallel to laminations; small compressional folds; and rotation structures are all also characteristic of ductile deformation during laminar flow (Fig. 7, LFA N3).

LFA S2 is interpreted to be the product of rapid subaqueous deposition by high-concentration channelized density flows (Rust and Romanelli, 1975; Rust, 1977; Cheel, 1982; Thomas, 1984; Mulder and Alexander, 2001; Bennett et al., 2002, 2006). Flow parallel imbrication of gravels at the base of LFA S2 indicates a high sediment concentration. Scouring at the base of the flow and rapid deposition of the poorly sorted clast-support coarse-grained material is indicated by the rip-up and incorporation of underlying pods of diamicton. A transition into crudely-stratified granule-gravel and sand indicates waning flow, while thin, interbedded diamicton beds with loaded upper contacts towards the top of LFA S2 are interpreted to record repeated subaqueous sediment gravity-flows by the downslope remobilization of outwash (Rust, 1977; Eyles et al., 1987; Plink-Björklund and Ronnert, 1999). Openwork gravels indicate periods of winnowing, possible close to the mouth of a channel. Thus, initially rapid scouring and deposition was followed by more episodic remobilization of material.

Syndepositional flow folds, including recumbent, isoclinal structures interpreted as fold noses (e.g. Stohl, LFA S1) (see Evenson, 1977; Hart and Roberts, 1994), and small open folds in front of dropstones (Fig. 10e) caused by flow down the palaeo-slope are interpreted to be the product of more cohesive debris flows (Piotrowski, 1994a). At Noer, the curving sand-filled lenses in LFA N2 are analogous to those observed in flow- or squeeze-till at Lake Erie Bluff (see Dreimanis, 1993), with the direction of lean imprinted by easterly flow (Fig. 6d). At Stohl, the sense of motion is further enhanced by gently undulating bedding interposed by massive diamicton beds, convolute sand rafts and channel fills (LFA S2) that are interpreted to reflect gravitational infilling of basins by flow lobes and channels (e.g. Phillips et al., 2008).

Our interpretation, of a sedimentary environment dominated by subaqueous density and debris flows, is consistent with the macrofabric data (Fig. 5). This is particularly clear at Stohl where clasts dip strongly down local palaeo-slopes (10–32°), towards the NE (F16, 15, 14, 12, 11) and SW (F9, 10). Girdle fabrics (F9, 10) are diagnostic of compression, while the range of strain signatures (S_1 values of 0.62–0.84) reflects locally variable flow. The lack of vertically-dipping clasts and the moderate to strong fabrics suggests rain-out was not significant or has been remobilized. A similar pattern is observed at Noer where clasts tend to dip NW, N and NE in the direction of the local palaeo-slope and other structural indicators (e.g. folds in front of dropstones), while girdle fabrics are commonplace (e.g. F3, F5 and F8). The range of strain signatures is even greater here (0.49–0.75) and there is a greater frequency of steeply dipping clasts, which suggests a larger component of rain-out.

6.2. Deposition in a proglacial glaciolacustrine environment (LFA A2)

The lithofacies at Altbülk are distinctive from those observed in Section 6.1. This includes, the presence of climbing ripples (Sr) indicating bottom current transport towards the NW (Jopling and Walker, 1968) and laminated silt–clay facies (Fl) that are interpreted as clastic varves (Fig. 15). Properties indicating varve deposition include rhythmic coarse (silt) and fine-grained (clay) couplets, with a sharp transition from clay to silt and a graded transition from silt to clay. The coarse component may therefore represent distal underflows into a lake basin during the summer months, while the fine-component is the settling of clay through the water column during winter quiescence (Smith and Ashley, 1985; Ringberg and Erlström, 1999; Palmer et al., 2008;

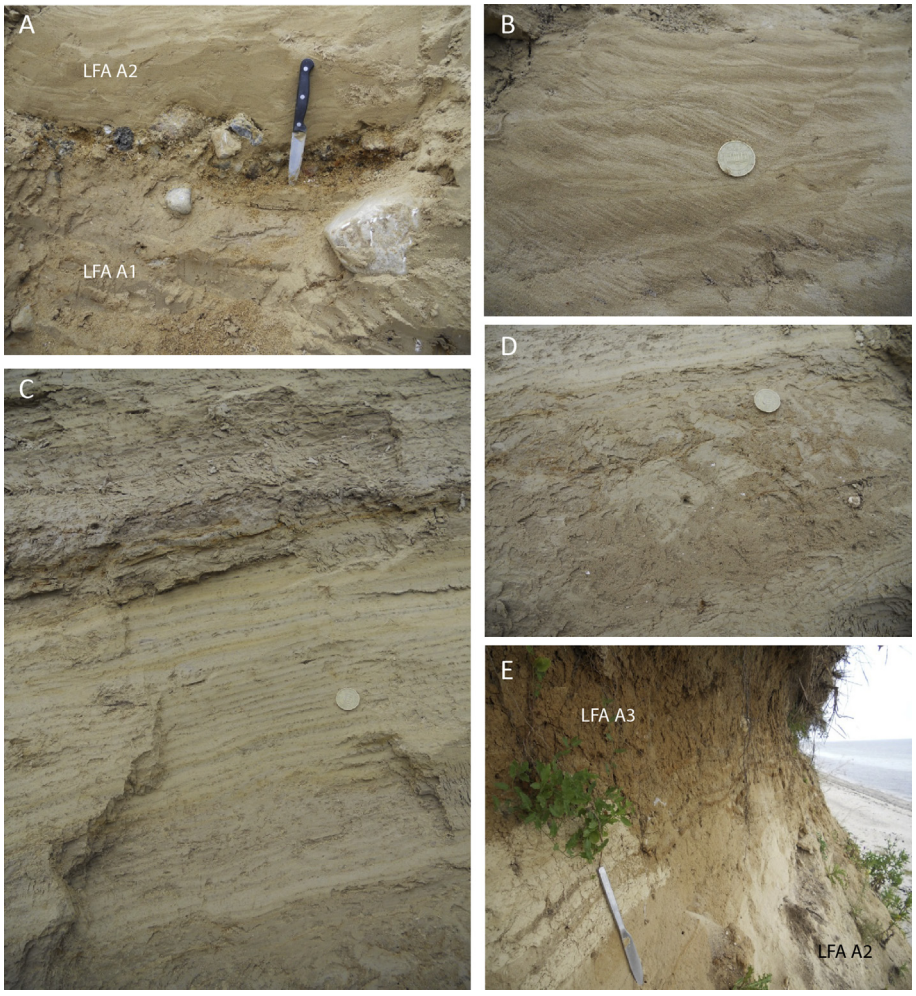

Fig. 14. Photographs of lithofacies exposed at Altbülk. A: Diamicton (LFA A1) overlain by clast-supported, imbricated gravel and then massive sand (LFA A2). B: Type-A climbing ripples recording a NW palaeo-current direction. Note the normal fault to the right of the coin. C: Laminated silt and clay facies (see Fig. 15 for micromorphology). D: Thin, brown clast-poor diamicton within the laminated silt and clay. Note the loaded upper contact. E: Transition from horizontally bedded sand into diamicton (LFA A3). The bottom half of the diamicton is characterised by horizontal inter-beds of granule-gravel, sand and silt.

Livingstone et al., 2010). The sharp contact between the winter laminae and succeeding summer laminae documents renewed transport of sediment into the lake.

6.3. Glacial deformation of lake sediments (LFA S1)

The clearest evidence for subglacial deformation is large amplitude glaciotectonic folding and rotation in LFA S1 (see also Hart et al., 1996; Piotrowski et al., 1994a). The large ~5 m high hook fold indicates ice-flow towards the NW. The deformation is partitioned within the lower part of LFA S1, with further undisturbed stratified diamicton draped on top. This is consistent with the identification of a lower subglacial deformation till (deformed section of LFA S1) (Hart et al., 1996), characterised as a grey, massive till folded together with waterlain sediments and comprising striated and faceted clasts and locally strong fabrics orientated ESE–WNW to SE–NW.

6.4. Subglacial till deposition (LFA N1, N4)

Whether or not the glaciolacustrine sediments are capped by a subglacial traction till (after Piotrowski, 1994a; Hart et al., 1996) is difficult to reconcile as there is no obvious transition and striated clasts are rare. Certainly LFA N4 becomes increasingly homogenized towards the top of the succession, which in combination with its continuity along the cliff face, strong (S_1: 0.68–0.75) and reasonably consistently N–S orientated macrofabrics (F1, 2, 6, 7), fissile character and presence of sheared/convoluted sand rafts suggests a subglacial till genesis (Evans et al., 2006a). At Altbülk both Piotrowski (1994a) and Hart et al. (1996) interpret the capping diamicton as a subglacial traction till due to evidence of deformation and/or truncation of underlying facies, although this was not observed during our investigation and is difficult to reconcile with the OSL chronology. It may instead relate to debris flow deposition during the melt-out of stagnant ice.

6.5. Grain size and lithology

Both the grain-size and lithological characteristics of the diamictons (Fig. 8) are fairly uniform within and between sites suggesting that the examined sections represent the same lithostratigraphical succession deposited by an ice sheet advancing from north-easterly direction. This is consistent with previous studies showing that this area was affected by the Young Baltic Ice Stream moving along the Baltic Sea depression at the end of the Weichselian glaciation (Stephan, 2001). The lack of systematic

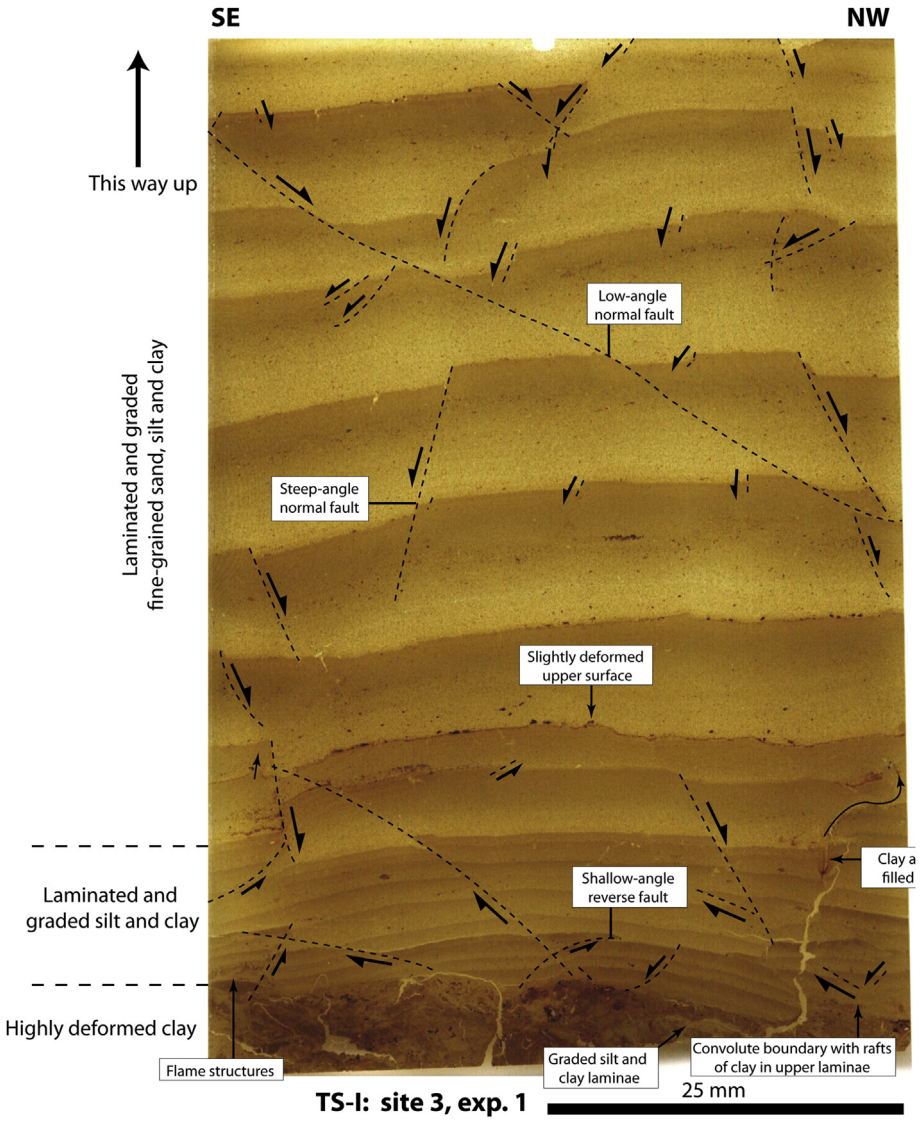

Fig. 15. Annotated scan of sample TS-I from Altbülk. This thin section is taken across the laminated sand and silt of LFA A2. Note the fining up from the coarse component into the fine component and the sharp upper contact of the fine component.

variations in fine-gravel composition and grain-size distribution suggests that multiple diamicton beds separated by sorted sediments should be explained by depositional processes rather than repeated ice advances and retreats. Differences in these characteristics may then be attributed to local sorting, winnowing and washing in a subaquatic environment. However, in nearby southern Denmark the provenance of diamictons has proven insufficient to differentiate between different ice advances (see Kjaer et al., 2003), and so this interpretation requires further testing.

7. Optically Stimulated Luminescence dating

Our results reveal a broad range of D_e distributions (Table 1, Fig. 16 and Supplementary Fig. 3). Samples shfd12083-12085 have broad unimodal peaks with low skew and OD when the outliers are removed. We therefore use CAM to derive D_e values for the final age calculations. Shfd12086, which was sampled from a waterlain diamicton, is skewed with a high OD (54%) and displays bimodal peaks. We interpret this as indicating some partial bleaching and therefore choose to use FMM taking the first component, which can explain 74% of the data. Samples Shfd12079, Shfd12081 and Shfd12082 show multi-modality, high OD (54%, 48% and 57% respectively) and skewing that would suggest partial bleaching and the use of MAM or the smallest FMM D_e component as most appropriate for age calculation purposes. In the case of Shfd12079 the MAM approach results in an unfeasibly young age (<14 ka) so our preference, given the stratigraphic context, is the FMM (dominant) component, which encompasses 64% of the data. For samples Shfd12081 and Shfd12082, both MAM and the smallest FMM D_e component resulted in very young ages (<12 ka). Therefore, for these samples a D_e value as calculated by CAM is our preference given our current understanding.

If stratigraphic context is ignored and the age models used are purely selected on the criteria of Bailey and Arnold (2006) and Boulter (2007) then the chronology for Altbülk is characterised by very young ages (8–15 ka) not in age order. If our preferred age models are used then we can achieve a more realistic deglacial chronology for LFA A2, with all the ages in the correct order. These result in an age of 19 ± 1.8 ka in rippled sand at the base of LFA A2, followed upwards by ages of 18.3 ± 2.2 ka and 16.7 ± 1.6 ka in waterlain diamicton and horizontally bedded sand respectively and finally 15.2 ± 1.3 ka from sand interbedded with diamicton. If these

results are accepted this would indicate deposition of LFA A2 over a period of ~4 ka giving sedimentation rates of ~12 mm yr^{-1}. This is consistent with the varve thicknesses (~10 mm) observed at LFA A2 (Fig. 15).

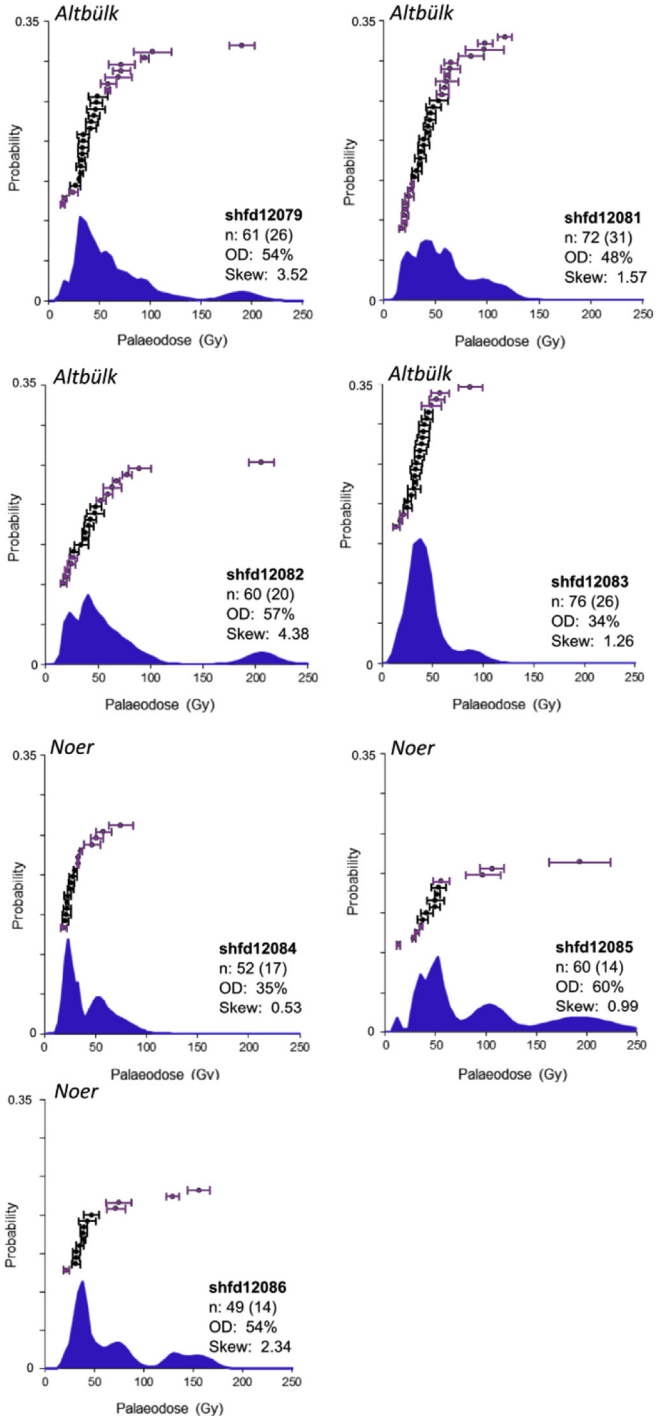

Fig. 16. Probability density function plots of D_e distributions for all samples. Overdispersion (OD), skew and n are also displayed. Based on our preferred age model (Table 1) palaeodoses we consider outliers (>2σ error) are shown in purple. Note there is no discernible difference between the two sites in terms of the probability density distributions. It is therefore difficult to determine whether the sediments were deposited subglacially or proglacially (Fig. 3). This may be because the time elapsed between the advance and retreat phases is only ~4 ka. (For interpretation of the references to colour in this figure legend, the reader is referred to the web version of this article.)

Luminescence ages from the intercalated waterlain diamicton, gravel, sand and clay beds of LFA N2 at Noer are more robust than for Altbülk, with two ages of ~23 ka (23.07 ± 2.3 and 23.13 ± 2.2) from waterlain diamicton and massive sand facies and another of 18.5 ± 1.5 ka from a deformed sand facies further to the east.

This chronology is significantly younger than Thermo-Luminescence (TL) ages of Marks et al. (1995), who sampled a range of sediments along the Dänischer Wohld Peninsula, including Stohl and Altbülk, and generated ages that clustered between 40 and 70 ka. However, as shown with this single grain data partial bleaching is thought to have been a significant issue for these sediment, something which the TL ages of Marks et al. (1995) could not have determined.

8. Discussion

The following discussion aims to determine whether the waterlain sediments on the Dänischer-Wohld Peninsula, northern Germany, were deposited in a subglacial or proglacial lake environment.

8.1. Altbülk

The simplest explanation for the glacigenic succession and OSL chronology at Altbülk is deposition in a proglacial lake dammed up against ice retreating into the Baltic Basin. In contrast to Noer and Stohl, sands and muds deposited by current transport (flow towards the NW) and suspended sediment settling comprise the bulk of the succession, while rainout of waterlain diamicton and dropstones are rare. The initial fining from gravel to rippled sand and then varved clay–silt is typical of an increasingly distal ice margin (Fig. 13). The varves indicate a seasonal control characteristic of proglacial lake sedimentation (e.g. Smith and Ashley, 1985). Indeed, varves are likely to be much rarer in subglacial lake settings (e.g. Livingstone et al., 2012), although hypothetically they could form due to seasonal supraglacial lake drainage events. Subsequent coarsening and the occurrence of diamicton debris-flows may indicate a minor re-advance of ice into the vicinity of the study area or more likely at this time period, debris flows associated with the melt-out of stagnant ice.

If our preferred age models are adopted (Table 1) the OSL dates at Altbülk produce a realistic deglacial chronology (e.g. Lüthgens et al., 2011; Houmark-Nielsen et al., 2012) in the correct age order. This would support a proglacial lake origin. The oldest OSL age of 19 ± 1.85 ka, taken from rippled sand at the base of the succession, is therefore interpreted as a minimum age for deglaciation of the Dänischer-Wohld Peninsula, northern Germany. An age of 15.2 ± 1.28 ka at the top of the succession constrains the lakes existence to about 4000 years. Given that the Dänischer Wohld Peninsula lies outside of the reconstructed high-stand of the Baltic Ice Lake and is associated with an earlier phase of deglaciation (see Björck, 1995; Jensen et al., 1997; Andrén et al., 2011), the lake most probably related to local ponding, dammed by stagnant ice topography.

8.2. Stohl and Noer

We suggest that the sites at Noer and Stohl record proglacial possibly followed by subglacial lake formation during advance of the Baltic Ice Stream to its maximum extent. Sedimentological and stratigraphic observations indicate a subaquatic subglacial or proglacial depositional environment dominated by rain-out of dropstone diamicton and mud, flow remobilization by subaqueous debris-flows and turbidity currents, and local sorting, winnowing and washing. The two ages of ~23 ka (23.07 ± 2.3 ka and

23.13 ± 2.2 ka) and another of 18.5 ± 1.5 ka taken at Noer are older than those at Altbülk and therefore thought to relate to an earlier event. Although there is no discernible difference in D_e distributions between the two sites (Fig. 16), the samples at Noer are characterised by fewer grains that passed the acceptance criteria, were less sensitive to dose and Shfd12085 contained a much larger percentage of saturated grains. This suggests at least some of the quartz was derived from a different sedimentary source and that some of the sediment had a different transport-deposition-burial pathway when compared to Altbülk (see Fig. 3). But we are unable to tell whether this relates to differences associated with proglacial vs subglacial deposition (Fig. 3). In northern Germany the ice sheet reached its maximum extent at ~22 ka BP (e.g. Houmark-Nielsen et al., 2003; Sommer and Benecke, 2009; Houmark-Nielsen, 2010; Ukkonen et al., 2011). The observed sedimentary succession of waterlain sediments capped by subglacial till is consistent with ice advance, and the two ~23 ka are within error and in agreement with the regional geochronology. We therefore accept the two ~23 ka ages, which constrain the waterlain sediments at Noer to (subglacial or proglacial) lake formation during ice advance.

The style of sedimentation and deformation offers a potential avenue for discriminating between former subglacial and proglacial lake environments. At both Noer and Stohl, the sedimentary succession is characterised by laminated/stratified diamicton intercalated with large lenses of tabular to channelized sorted sediments (LFA N2-3, S1-2). Such a vertically stacked sedimentary succession has been ascribed to aggradation within subglacial lakes or cavities where the accommodation space is restricted (Munro-Stasiuk, 1999; Wysota, 2007; Clerc et al., 2012; Ravier et al., 2014a). In contrast, prograding sedimentary structures that are typical of proglacial environments (e.g. Ravier et al., 2014a) are largely absent at the two sites. Indeed, one might expect an upward coarsening or fining architecture if deposition was into a proglacial lake from an advancing of retreating ice mass. The transition from sorted sediments (LFA N2-3) into subglacial till (LFA N4) at Noer suggests a common subglacial depositional environment, possibly associated with a gradual switch from subaqueous deposition to localised deformation (ductile and then brittle) and till aggradation following ice-bed recoupling.

Contrary to other sedimentary successions ascribed to subglacial sheet, cavity or lake formation, there is limited sedimentary or deformational evidence (hydroplastic deformation, fluidization and hydrofracturing of discrete sediment layers) for repeated (de) coupling of the ice-bed due to drainage events or fluctuations in subglacial meltwater pressure (Piotrowski and Tulaczyk, 1999; Boyce and Eyles, 2000; Piotrowski et al., 2001; Phillips et al., 2007, 2008; Wysota, 2007; Lesemann et al., 2010; Clerc et al., 2012; Ravier et al., 2014a,b). The waterlain sediments are relatively undisturbed, apart from two 1–2 m layers at Noer where discrete sediment packages have been highly disturbed and fluidized, most likely due to remobilization as density flows (Gravenor et al., 1984), and the lower part of the sediments at Stohl, which have been proglacially glaciotectonised and overridden (see below). The identification of thin, undeformed stringers of intra-till sorted sediments attributed to basal meltwater washing during phases of ice-bed separation (e.g. Piotrowski and Tulaczyk, 1999; Boyce and Eyles, 2000; Piotrowski et al., 2001; Wysota, 2007) have been observed along the Baltic Coast (e.g. Piotrowski and Tulaczyk, 1999), indicating an environment dominated by high water pressures, ice-bed decoupling and basal sliding. Although the juxtaposition of sorted sediment and diamicton is analogous to these ice-bed separation features, the absence of intra-till beds or discrete deformation zones could either imply proglacial sedimentation or a subglacial environment that remained decoupled for an extended period of time. Certainly, subglacial lakes are not thought to completely empty during drainage events (Pattyn, 2008) and may therefore be associated with persistent ice-bed decoupling. Multiple phases of (de)coupling are more indicative of ephemeral subglacial drainage systems or small cavities (e.g. Lesemann et al., 2010; Clerc et al., 2012; Narloch et al., 2012, 2013; Tylmann et al., 2013; Ravier et al., 2014a).

At Stohl, towards the bottom of the succession, the waterlain sediments have been subjected to localised large-amplitude, asymmetric glaciotectonic folding and rotation (Figs. 9 and 10d,h). This is interpreted to record proglacial deformation and glacial overriding of a proglacial lake sequence during advance of the Baltic Ice Stream to its maximum limits (see also Hart et al., 1996; Piotrowski, 1994). High-amplitude (>5 m) folding and glaciotectonic stacking is typically, although not exclusively (e.g. Phillips et al., 2007), associated with deformation in an unconfined proglacial environment (e.g. Roberts and Hart, 2005; Phillips et al., 2008; Ó Cofaigh et al., 2011). The orientation of the hook fold suggests ice flow towards the NW, consistent with the ESE–WNW to SE–NW orientated fabrics recorded by Hart et al. (1996) . Significantly, the glaciotectonised sediment package is draped by further, undisturbed waterlain sediments analogous to those observed at Noer. These sediments could either have been deposited subglacially, in an aqueous environment after ice overrode the Peninsula, or in a proglacial lake formed during ice retreat into the Baltic Basin. Although the top of the cliffs were difficult to access while we were there, Piotrowski (1992) previously interpreted the top unit as a flow till. This could have resulted from glaciofluvial, glaciolacustrine and debris-flow deposition between stagnant and melting ice masses that also generated the hummocky moraine in Schleswig–Holstein (Fig. 2).

A key consideration is whether the undisturbed waterlain sediments at Noer and Stohl were deposited during the same event. If so, then the ~23 ka OSL ages from Noer preclude proglacial lake formation in-front of a retreating ice-margin because the Baltic Ice Stream was still advancing to its maximum limits during this time. In this scenario, the simplest interpretation is deposition in a subglacial lake; the OSL ages then represent an inherited signal of proglacial lake deposition during ice advance (Fig. 3a,b). If they are not contiguous it becomes more difficult to distinguish between a proglacial and subglacial origin. Stratigraphically, the undisturbed waterlain sediments at Noer and Stohl are both sandwiched between more homogenous and pervasive diamicton facies, although ultimately ages are needed from Stohl to confirm whether they are part of the same sequence. However, a subglacial depositional model is currently favoured given: (i) the presence of laminated/stratified diamicton intercalated with large lenses of tabular to channelized sorted sediments (LFA N2-3, S1 & A1), indicating aggradation by density flows, current reworking and rain out in a confined environment (e.g. Munro-Stasiuk, 1999; Wysota, 2007; Clerc et al., 2012; Ravier et al., 2014a); (ii) the transition from waterlain sediment into subglacial till at Noer, indicative of a common depositional environment; (iii) the absence of ice-marginal glaciotectonic thrusting and folding associated with overridden proglacial environments (e.g. . Roberts and Hart, 2005; Phillips et al., 2008; Ó Cofaigh et al., 2011); (iv) the absence of progradation structures and upwards fining or coarsening of the waterlain sediments that typify retreating and advancing ice-margins respectively (Ravier et al., 2014a); and (v) identification of tunnel valleys radiating southwards from the study sites (Fig. 2), which provide geomorphological support for the periodic drainage of stored subglacial meltwater to the ice margin (Livingstone et al., 2012; and see also Piotrowski, 1994b). Borehole data from the Bornhöved tunnel valley region, ~40 km to the south of our study area, indicates that the final phase of tunnel valley incision relates to Late Weichselian ice flow. High-energy outburst of subglacial

water is evidenced by the deposition of the Kalübbe Sandur and Trappenkamp gravel beds at the southern extension of the Bornhöved tunnel valley (Piotrowski, 1994b).

8.3. Implications for ice-sheet dynamics and lake formation in northern Germany

Irrespective of whether a proglacial or subglacial model is adopted for the undisturbed waterlain sediments at Noer and Stohl, the OSL ages constrain two major phases of ice activity in Schleswig–Holstein: (1) advance of the Baltic Ice Stream across the study area at ~23 ka resulting in formation of a proglacial lake along the margin of the Dänischer Wohld Peninsula; and (2) final retreat of ice back into the Baltic Basin at ~19 ka and formation of an ice-dammed lake that persisted for ~4000 years. Given the reconstructed high-stand and timing of the Baltic Ice Lake and the deglacial chronology of the southwestern Baltic Basin (e.g. Bjorck, 1995; Jensen et al., 1997), lake formation is likely to have been localised and possibly dammed by stagnant ice topography. In addition, we suggest that at Stohl and Noer there is evidence for subglacial lake formation along the margin of the Baltic Basin between 23 and 19 ka. The relative sizes of the former pro- and subglacial lakes are difficult to determine given the limited spatial information constraining the distribution of waterlain deposits. However, Noer and Stohl are ~10 km apart and so if the waterlain sediments were contiguous then the implication is that a substantial subglacial water body >10 km in length existed. The drainage of water stored in such a lake provides a mechanism for erosion of the N–S orientated tunnel valleys and the emplacement of gravels and sandur deposits by high-energy outbursts.

8.4. Implications for discriminating between subglacial and proglacial lakes

The results of this study demonstrate the difficulty in discriminating between subglacial and proglacial lake sediments deposited by a similar set of processes (e.g. Livingstone et al., 2012). This necessitates the use of multiple discriminating tools, including geomorphological, sedimentological and dating methods. Although there is no one method or diagnostic criterion that allows for the conclusive identification of a palaeo-subglacial lake, we found certain tools to be more useful than others.

The style of sedimentation and deformation offers one means of differentiating overridden proglacial lake sediments from subglacial lake sediments. In particular, progressive proglacial to subglacial deformation, as observed at the base of LFA S1, is typically characterised by large-scale compressive glaciotectonic thrusting and folding of the glaciolacustrine sequence (e.g. Evans et al., 2006a; Phillips et al., 2008), resulting in a thick sediment stack with an increasing strain history (Ó Cofaigh et al., 2011). Conversely, subglacial waterlain sediments deposited during periods of ice-bed decoupling (thin water films to subglacial lakes) may be preserved due to passive melt-out of sediments and net till aggradation, or by the partitioning of ductile deformation, fluidization and hydrofracturing within discrete water-lubricated sediment packages (e.g. Evans et al., 2006b; Phillips et al., 2007, 2008; Lesemann et al., 2010; Clerc et al., 2012; Ravier et al., 2014a). Subglacial aquatic environments are typically thought to produce conformably stacked stratified/laminated diamicton and tabular to channelized sorted gravel, sand and mud deposited by density flows, rain out and current reworking processes (e.g. Munro-Stasiuk, 1999; Ravier et al., 2014a). Progradation structures and fining/coarsening architectures are likely to be absent due to the limited accommodation space and position of subglacial lakes beneath the ice rather than proximal or distal to an advancing or retreating ice margin.

Luminescence palaeodose distributions based on single grain measurements offer a potentially powerful method for fingerprinting sediment transport and depositional histories. This is because the luminescence signal in a proglacial environment will vary depending upon its depositional pathway, while a subglacial lake will retain an inherited signature of events prior to deposition (Fig. 3). However, the variable response of quartz grains and the wide range of conditions and sediment transport pathways in both proglacial and subglacial settings (e.g. Fuchs and Owen, 2008) give great scope for complexity and overlap as shown by our results. Further work is therefore required to fingerprint the influence of depositional processes on the luminescence signal of modern and ancient glaciolacustrine sediments. This will allow better discrimination of, for example, *in situ* and subglacially cannibalized proglacial lake sediments (Fig. 3b).

9. Conclusions

The widespread existence of subglacial lakes beneath contemporary ice masses, and their predicted existence beneath palaeo-ice sheets, necessitates a re-appraisal of the automatic interpretation of glaciolacustrine sediments as proglacial in origin. The onus should be on demonstrating rather than presuming a proglacial origin. Indeed, we hypothesise that numerous deposits currently interpreted to record proglacial lake sedimentation may actually have been deposited by their subglacial cousins. However, there is no incontrovertible method for discriminating subglacial lake sediments in the geological record. This makes it a difficult problem that requires a closer examination of reputed palaeo-subglacial lake sites to tease out diagnostic criteria, and the development of techniques or multi-disciplinary approaches to improve our discriminating skill.

In this paper we tackled the problem by investigating sites along the Dänischer Wohld Peninsula, northern Germany, which have been conflictingly interpreted to record deposition in both proglacial and subglacial aqueous environments. We identified two major phases of ice activity and associated lake formation during the Late Weichselian glaciation. (1) Initial advance of the Baltic Ice Stream across the Dänischer Wohld Peninsula at ~23 ka. This resulted in formation of a proglacial lake along the edge of the Baltic Basin that was subsequently overridden and the sediments glaciotectonised as ice advanced across it. (2) Retreat of ice back into the Baltic Basin at ~19 ka and formation of an ice-dammed proglacial lake that persisted for ~4000 years.

An additional phase of subglacial lake activity may have occurred at two of the sites following advance of ice to its maximum extent between 23 and 19 ka. This inference is based on the style of sedimentation, which is consistent with other inferred subglacial aquatic environments, the juxtaposition of relatively undeformed waterlain sediment and subglacial till, absence of glaciotectonic thrusting and folding or of fining/coarsening successions and the geomorphic association with tunnel valleys to the south of the study area.

Of the discriminating tools used in this study, the style of sedimentation and deformation proved the most useful for distinguishing between subglacial and proglacial depositional environments. In addition, the luminescence signal palaeodose distributions offer a potentially powerful means of fingerprinting sediment transport pathways of young systems, although further work is required.

Acknowledgements

This work was supported by a NERC Early Career Research Fellowship awarded to SJL (NE/H015256/1). We are grateful to the

logistical support of Klaus Schwarzer and Eckart Bedbur. Karen Luise Knudsen carried out the micropalaeontological investigation and Robert Ashurt helped prepare the OSL samples. We thank Chris and Kathy Denison for funding the PhD of JCE. The authors wish to thank Jutta Winsemann and an anonymous reviewer for informative and helpful reviews.

Appendix A. Supplementary data

Supplementary data related to this article can be found at http://dx.doi.org/10.1016/j.quascirev.2015.01.030.

References

Alexanderson, H., Murray, A.S., 2012. Problems and potential of OSL dating Weichselian and Holocene sediments in Sweden. Quat. Sci. Rev. 44, 37–50.
Andrén, T., Björck, S., Andrén, E., Conley, D., Zillén, L., Anjar, J., 2011. The development of the Baltic Sea Basin during the last 130 ka. In: The Baltic Sea Basin. Springer Berlin Heidelberg, pp. 75–97.
Anjar, J., Larsen, N.K., Håkansson, L., Möller, P., Linge, H., Fabel, D., Xu, S., 2014. A ^{10}Be-based reconstruction of the last deglaciation in southern Sweden. Boreas 43, 132–148.
Arnold, L.J., Roberts, R.G., 2009. Stochastic modelling of multi-grain equivalent dose (De) distributions: implications for OSL dating of sediment mixtures. Quat. Geochronol. 4, 204–230.
Bailey, R.M., Arnold, L.J., 2006. Statistical modelling of single grain quartz De distributions and an assessment of procedures for estimating burial dose. Quat. Sci. Rev. 25, 2475–2502.
Bateman, M.D., Frederick, C.D., Jaiswal, M.K., Singhvi, A.K., 2003. Investigations into the potential effects of pedoturbation on luminescence dating. Quat. Sci. Rev. 22, 1169–1176.
Bateman, M.D., Boulter, C.H., Carr, A.S., Frederick, C.D., Peter, D., Wilder, M., 2007. Preserving the palaeoenvironmental record in Drylands: bioturbation and its significance for luminescence-derived chronologies. Sediment. Geol. 195, 5–19.
Bateman, M.D., Buckland, P.C., Whyte, M.A., Ashurst, R.A., Boulter, C., Panagiotakopulu, E., 2011. Re-evaluation of the Last Glacial Maximum typesite at Dimlington, UK. Boreas 40, 573–584.
Bateman, M.D., Hitchens, S., Murton, J.B., Lee, J.R., Gibbard, P.L., 2014. The evolution of periglacial patterned ground in East Anglia, UK. J. Quat. Sci. 29, 301–317.
Bennett, M.R., Huddart, D., Thomas, G.S.P., 2002. Facies architecture within a regional glaciolacustrine basin: Copper River, Alaska. Quat. Sci. Rev. 21, 2237–2279.
Bennett, M.R., Huddart, D., Waller, R.I., 2006. Diamict fans in subglacial water-filled cavities – a new glacial environment. Quat. Sci. Rev. 25, 3050–3069.
Bentley, M.J., Christoffersen, P., Hodgson, D.A., Smith, A.M., Tulaczyk, S., Le Brocq, A.M., 2011. Subglacial lake sedimentary processes: potential archives of ice sheet evolution, past environmental change and the presence of life. In: Siegert, M.J., Kennicutt, C., Bindschadler, B. (Eds.), Subglacial Antarctic Aquatic Environments. AGU Monograph.
Björck, S., 1995. A review of the history of the Baltic Sea, 13.0–8.0 ka BP. Quat. Int. 27, 19–40.
Boulter, C.H., 2007. Reconstructing the Palaeoenvironmental Dynamics of East Central Texas since the Last Glacial Maximum (PhD thesis). University of Sheffield.
Boyce, J.I., Eyles, N., 2000. Architectural element analysis applied to glacial deposits: internal geometry of a late Pleistocene till sheet, Ontario, Canada. Bull. Geol. Soc. Am. 112, 98–118.
Carrivick, J.L., Tweed, F.S., 2013. Proglacial lakes: character, behaviour and geological importance. Quat. Sci. Rev. 78, 34–52.
Cheel, R.J., 1982. The depositional history of an esker near Ottawa, Canada. Can. J. Earth Sci. 19, 1417–1427.
Christoffersen, P., Tulaczyk, S., Wattrus, N.J., Peterson, J., Quintana-Krupinski, N., Clark, C.D., Sjunneskog, C., 2008. Large subglacial lake beneath the Laurentide Ice Sheet inferred from sedimentary sequences. Geology 36, 563–566.
Clerc, S., Buoncristiani, J.-F., Guiraud, M., Desaubliaux, G., Portier, E., 2012. Depositional model in subglacial cavities, Killiney Bay, Ireland. Interactions between sedimentation, deformation and glacial dynamics. Quat. Sci. Rev. 33, 142–164.
Cunningham, A.C., Wallinga, J., 2010. Selection of integration time intervals for quartz OSL decay curves. Quat. Geochronol. 5 (6), 657–666.
Dreimanis, A., 1993. Small to medium-sized glacitectonic structures in till and in its substratum and their comparison with mass movement structures. Quat. Int. 18, 69–79.
Ehlers, J., Wingfield, R., 1991. The extension of the Late Weichselian/Late Devensian ice sheets in the North Sea Basin. J. Quat. Sci. 6, 313–326.
Evans, D.J.A., Benn, D.I., 2004. A Practical Guide to the Study of Glacial Sediments. Edward Arnold, London.
Evans, D.J.A., Phillips, E.R., Hiemstra, J.F., Auton, C.A., 2006a. Subglacial till: formation, sedimentary characteristics and classification. Earth-Sci. Rev. 78, 115–176.
Evans, D.J.A., Rea, B.R., Hiemstra, J.F., Ó Cofaigh, C., 2006b. A critical assessment of the subglacial megafloods: a case study of glacial sediments and landforms in south-central Alberta, Canada. Quat. Sci. Rev. 25, 1638–1667.
Evatt, G.W., Fowler, A.C., Clark, C.D., Hulton, N.R.J., 2006. Subglacial floods beneath ice sheets. Philos. Trans. R. Soc. Lond. Ser. A 374, 1769–1794.
Evenson, E.B., Dreimanis, A., Newsom, J.W., 1977. Subaquatic flow tills: a new interpretation for the genesis of some laminated till deposits. Boreas 6, 115–133.
Eyles, N., 1987. Late Pleistocene debris-flow deposits in large glacial lakes in British Columbia and Alaska. Sediment. Geol. 53, 33–71.
Eyles, N., Clark, B.M., Clague, J.J., 1987. Coarse-grained sediment gravity flow facies in a large supraglacial lake. Sedimentology 34, 193–216.
Eyles, N., Eyles, C.H., McCabe, A.M., 1989. Sedimentation in an ice-contact subaqueous setting: the Middle-Pliestocene 'North Sea Drfits' of Norfolk, U.K. Quat. Sci. Rev. 8, 57–74.
Fuchs, M., Owen, L.A., 2008. Luminescence dating of glacial and associated sediments: review, recommendations and future directions. Boreas 37, 636–659.
Galbraith, R.F., Green, P.F., 1990. Estimating the component ages in a finite mixture. International Journal of Radiation Applications and Instrumentation. Part D. Nucl. Tracks Radiat. Meas. 17, 197–206.
Galbraith, R.F., Roberts, R.G., Laslett, G.M., Yoshida, H., Olley, J.M., 1999. Optical dating of single and multiple grains of quartz from Jinmium rock shelter, northern Australia. Part 1. Experimental design and statistical models. Archaeometry 41, 339–364.
Gibbard, P., 1980. The origin of the stratified Catfish Creek Till by basal melting. Boreas 9, 71–85.
Gjessing, J., 1960. Isavsmeltningstidens drenering, dens forløp og formdannende virkning i nordre Atnedalen. Med sammenlignende studier fra nordre Gudbrandsdalen og nordre Østerdalen. In: Ad Novas, no. 3. Oslo Universitetsforlaget.
Gravenor, C.P., von Brunn, V., Dreimanis, A., 1984. Nature and classification of waterlain glaciogenic sediments exemplified by Pleistocene, Late Palaeozoic and Late Precambrian deposits. Earth-Science Rev. 20, 105–166.
Hart, J.K., Roberts, D.H., 1994. Criteria to distinguish between subglacial glaciotectonic and glaciomarine sedimentation, I. Deformation styles and sedimentation. Sediment. Geol. 91, 191–213.
Hart, J.K., Gane, F., Watts, R.J., 1996. Deforming bed conditions on the Dänischer Wohld Peninsula, northern Germany. Boreas 25, 101–113.
Hart, J.K., Gane, F., Watts, R.J., 1997. 'Deforming bed conditions on the Dänischer Wohld Peninsula, northern Germany': reply to comments. Boreas 26, 79–80.
Hoaglin, D.C., Mosteller, F., Tukey, J.W., 1983. Understanding Robust, Exploratory Data Analysis. Wiley, Chichester, p. 447.
Houmark-Nielsen, M., 2010. Extent, age and dynamics of Marine Isotope Stage 3 glaciations in the southwestern Baltic Basin. Boreas 39, 343–359.
Houmark-Nielsen, M., Kjaer, K.H., 2003. Southwest Scandinavia, 40–15 kyr BP: palaeogeography and environmental change. J. Quat. Sci. 18, 769–786.
Houmark-Nielsen, M., Linge, H., Fabel, D., Schnabel, C., Xu, S., Wilcken, K.M., Binnie, S., 2012. Cosmogenic surface exposure dating the last deglaciation in Denmark: discrepancies with independent age constraints suggest delayed periglacial landform stabilisation. Quat. Geochronol. 13, 1–17.
Jensen, J.B., Bennike, O., Witkowski, A., Lemke, W., Kujpers, A., 1997. The Baltic Ice Lake in the southwestern Baltic: sequence-, chrono- and biostratigraphy. Boreas 26, 217–236.
Jopling, A.V., Walker, R.G., 1968. Morphology and origin of ripple-drift cross-laminations, with examples from the Pleistocene of Massachusetts. J. Sediment. Petrol. 38, 971–984.
Jørgensen, F., Piotrowski, J.A., 2003. Signature of the Baltic Ice Stream on Funen Island, Denmark during the Weichselian glaciation. Boreas 32, 242–256.
Kjaer, K.H., Houmark-Nielsen, M., Richardt, N., 2003. Ice-flow patterns and dispersal of erratics at the southwestern margin of the last Scandinavian Ice Sheet: signature of palaeo-ice streams. Boreas 32, 130–148.
Kronborg, C., 1986. Fine gravel content in tills. Aarhus Geoskrifter 24, 189–210.
Lachniet, M.S., Larson, G.J., Strasser, J.C., Lawson, D.E., Evenson, E.B., 1999. Microstructures of glacigenic sediment flow deposits, Matanuska Glacier. In: Mickelson, D.M., Attig, J.W. (Eds.), Glacial Processes Past and Present, Geological Society of America, Special Paper 337, pp. 45–57. Boulder CO.
Lachniet, M.S., Larson, G.J., Lawson, D.E., Evenson, E.B., Alley, R.B., 2001. Microstructure of sediment flow deposits and subglacial sediments: a comparison. Boreas 30, 254–262.
Larsen, E., Kjaer, K., Demidov, I.N., Funder, S., Grøsfjeld, K., Houmark-Nielsen, M., Jensen, M., Linge, H., Lysså, A., 2006. Late Pleistocene glacial and lake history of northwestern Russia. Boreas 35, 394–424.
Larsen, N.K., Knudsen, K.L., Krohn, C.F., Kronborg, C., Murray, A.S., Nielsen, O.B., 2009. Late Quaternary ice sheet, lake and sea history of southwest Scandinavia – a synthesis. Boreas 38, 732–761.
Lee, J.R., Phillips, E.R., 2008. Progressive soft sediment deformation within a subglacial shear zone – a hybrid mosaic – pervasive deformation model for Middle Pleistocene glaciotectonised sediments from Eastern England. Quat. Sci. Rev. 27, 1350–1362.
Lesemann, J.-E., Alsop, G.I., Piotrowski, J.A., 2010. Incremental subglacial sediment deposition and deformation associated with repeated ice-bed decoupling: a case study form the Island of Funen, Denmark. Quat. Sci. Rev. 29, 3212–3229.
Livingstone, S.J., Ó Cofaigh, C., Evans, D.J.A., 2010. Sedimentary evidence for a major glacial oscillation and proglacial lake formation in the Solway Lowlands (Cumbria, UK) during the Late Devensian deglaciation. Boreas 39, 505–527.

Livingstone, S.J., Clark, C.D., Piotrowski, J.A., Tranter, M.J., Bentley, M.J., Hodson, A., Swift, D.A., Woodward, J., 2012. Theoretical framework and diagnostic criteria for the identification of palaeo-subglacial lakes. Quat. Sci. Rev. 55, 88–110.
Livingstone, S., Clark, C., Tarasov, L., 2013. Modelling North American palaeo-subglacial lakes and their meltwater drainage pathways. Earth Planet. Sci. Lett. 375, 13–33.
Lundqvist, J., Wohlfarth, B., 2001. Timing and east-west correlation of south Swedish ice marginal lines during the Late Weichselian. Quat. Sci. Rev. 20, 1127–1148.
Lüthgens, C., Böse, M., Preusser, F., 2011. Age of the Pomeranian ice-marginal position in northeastern Germany determined by Optically Stimulated Luminescence (OSL) dating of glaciofluvial sediments. Boreas 40, 598–615.
Marks, L., Piotrowski, J.A., Stephan, H.-J., Fedorowicz, S., Butrym, J., 1995. Thermoluminescence indications of the Middle Weichselian (Vistulian) Glaciation in northwest Germany. Meyniana 47, 69–82.
McCabe, A.M., Ó Cofaigh, C., 1994. Sedimentation in a subglacial lake, Enniskerry, eastern Ireland. Sediment. Geol. 91, 57–95.
Medialdea, A., Thomsen, K.J., Murray, A.S., Benito, G., 2014. Reliability of equivalent-dose determination and age-models in the OSL dating of historical and modern palaeoflood sediments. Quat. Geochronol. 22, 11–24.
Mulder, T., Alexander, J., 2001. The physical character of subaqueous sedimentary density flows and their deposits. Sedimentology 48, 269–299.
Munro-Stasiuk, M.J., 1999. Evidence for water storage and drainage at the base of the Laurentide ice sheet, south-central Alberta, Canada. Ann. Glaciol. 28, 175–180.
Murray, A.S., Wintle, A.G., 2000. Luminescence dating of quartz using an improved single-aliquot regenerative-dose protocol. Radiat. Meas. 32, 57–73.
Murray, A.S., Wintle, A.G., 2003. The single-aliquot regenerative-dose protocol: potential for improvements in reliability. Radiat. Meas. 37, 377–381.
Narloch, W., Piotrowski, J.A., Wysota, W., Larsen, N.K., Menzies, J., 2012. The signature of strain magnitude in tills associated with the Vistula Ice Stream of the Scandinavian Ice Sheet, central Poland. Quat. Sci. Rev. 57, 105–120.
Narloch, W., Wysota, W., Piotrowski, J.A., 2013. Sedimentological record of subglacial conditions and ice sheet dynamics of the Vistula Ice Stream (north-central Poland) during the Last Glaciation. Sediment. Geol. 293, 30–44.
Ó Cofaigh, C., Evans, D.J.A., Hiemstra, J.F., 2011. Formation of a stratified subglacial 'till' assemblage by ice-marginal thrusting and glacier overriding. Boreas 40, 1–14.
Palmer, A.P., Rose, J., Lowe, J.J., Walker, M.J.C., 2008. Annually laminated Late Pleistocene sediments from Llangorse Lake, South Wales: a chronology for the pattern of ice wastage. Proc. Geol. Assoc. 119, 245–258.
Pattyn, F., 2008. Investigating the stability of subglacial lakes with a full Stokes ice-sheet model. J. Glaciol. 54, 353–361.
Phillips, E.R., Merritt, J., Auton, C., Golledge, N.R., 2007. Microstructures in subglacial and proglacial sediments: understanding faults, folds and fabrics, and the influence of water on the style of deformation. Quat. Sci. Rev. 26, 1499–1528.
Phillips, E.R., Lee, J.R., Burke, H., 2008. Progressive proglacial to subglacial deformation and syntectonic sedimentation at the margins of the Mid-Pleistocene British Ice Sheet: evidence from north Norfolk, UK. Quat. Sci. Rev. 27, 1848–1871.
Piotrowski, J.A., 1992. Till facies and depositional environments of the upper sedimentary complex from the Stohler Cliff, Schleswog-Holstein, North Germany. Z. Geomorphol. N. F. Supp.-Bd 84, 37–54.
Piotrowski, J.A., 1994a. Waterlain and lodgement till facies of the lower sedimentary complex from the Dänischer Wohld Peninsula, North Germany. In: Warren, W.P., Croot, D. (Eds.), Formation and Deformation of Glacial Deposits. Balkema, Rotterdam, pp. 3–8.
Piotrowski, J.A., 1994b. Tunnel-valley formation in northwest Germany – geology, mechanisms of formation and subglacial bed conditions for the Bornhöved Tunnel Valley. Sediment. Geol. 89, 107–141.
Piotrowski, J.A., 1996. Dynamik und subglaziale Paläohydrogeologie der weichselzeitlichen Eiskappe in Zentral-Schleswig-Holstein. Berichte-Rep. Geol. Paläontol. Inst. Univ. Kiel 79, 188.
Piotrowski, J.A., 1997. Subglacial groundwater flow during the last glaciation in northwestern Germany. Sediment. Geol. 111, 217–224.
Piotrowski, J.A., Tulaczyk, S., 1999. Subglacial conditions under the last ice sheet in northwest Germany: ice-bed separation and enhanced basal sliding? Quat. Sci. Rev. 18, 737–751.
Piotrowski, J.A., Döring, U., Harder, A., Qadirie, R., Wegenhöfer, S., 1997. 'Deforming bed conditions on the Dänischer Wohld Peninsula, northern Germany': comments. Boreas Comments 26, 73–77.
Piotrowski, J.A., Mickelson, D.M., Tulaczyk, S., Krzyszowski, D., Junge, F.W., 2001. Were deforming bed beneath past ice sheets really widespread? Quat. Int. 86, 139–150.
Plink-Björklund, P., Ronnert, L., 1999. Depositional processes and internal architecture of Late Weichselian ice-marginal submarine fan and delta settings, Swedish west coast. Sedimentology 46, 291–294.
Prange, W., 1987. Gefügekundliche Untersuchungen der weichselzeitlichen Ablagerungen an den Stilufern des Dänischen Wohlds, Schleswig-Holstein. Meyniana 39, 85–110.
Prange, W., 1990. Glazialgeologische Aufschlu ßuntersuchungen im weichselzeitlichen Vereisungsgebiet zwischen Schleswig und Kiel. Meyniana 42, 65–92.
Prescott, J.R., Hutton, J.T., 1994. Cosmic ray contributions to dose rates for luminescence and ESR dating: large depths and long-term variations. Radiat. Meas. 23, 497–500.
Preusser, F., 1999. Lumineszenzdatierung fluviatiler Sedimente; Fallbeispiele aus der Schweiz und Norddeutschland. In: Kölner Forum für Geologie and Paläontologie 3, pp. 1–62.
Ravier, E., Buoncristiani, J.-F., Clerc, S., Guiraud, M., Menzies, J., Portier, E., 2014a. Sedimentological and deformational criteria for discriminating subglaciofluvial deposits from subaqueous ice-contact fan deposits: a Pleistocene example (Ireland). Sedimentology 61, 1382–1410.
Ravier, E., Buoncristiani, J.-F., Guiraud, M., Menzies, J., Clerc, S., Goupy, B., Portier, E., 2014b. Porewater pressure control on subglacial soft sediment remobilization and tunnel valley formation; A case study from the Alnif tunnel valley (Morocco). Sediment. Geol. 304, 71–95.
Rebesco, M., Camerlenghi, A., De Santis, L., Domack, E., Kirby, M., 1998. Seismic stratigraphy of Palmer Deep: a fault-bounded late Quaternary sediment trap on the inner continental shelf, Antarctic Peninsula Pacific margin. Mar. Geol. 151, 89–110.
Rhodes, E.J., 2007. Quartz single grain OSL sensitivity distributions: implications for multiple grain single aliquot dating. Geochronometria 26, 19–29.
Ringberg, B., Erlström, M., 1999. Micromorphology and petrography of Late Weichselian glaciolacustrine varves in southeastern Sweden. Catena 35, 147–177.
Roberts, D.H., Hart, J.K., 2005. The deforming bed characteristics of a stratified till assemblage in north east East Anglia, UK: investigating controls on sediment rheology and strain signatures. Quat. Sci. Rev. 24, 123–140.
Russell, H.A.J., Arnott, R.W.C., 2003. Hydraulic-jump and hyperconcentrated-flow deposits of a glacigenic subaqueous fan: Oak Ridges Moraine, Southern Ontario, Canada. J. Sediment. Res. 73, 887–905.
Rust, B.R., 1977. Mass flow deposits in a Quaternary succession near Ottawa, Canada: diagnostic criteria for subaqueous outwash. Can. J. Earth Sci. 14, 175–184.
Rust, B.R., Romanelli, R., 1975. Late Quaternary subaqueous outwash deposits near Ottawa, Canada. In: Jopling, A.V., McDonald, B.C. (Eds.), Glaciofluvial and Glaciolacustrine Sedimentation, Society of Economic Paleontologists and Mineralogists, Special Publication 23, pp. 177–192.
Smith, N.D., Ashley, G.M., 1985. Proglacial lacustrine environment. In: Ashley, G.M., Shaw, J., Smith, N.D. (Eds.), Glacial Sedimentary Environments 135–212Society of Palaeontologists and Mineralogists, Tulsa.
Sommer, R.S., Benecke, N., 2009. First radiocarbon dates on wooly mammoth (*Mammuthus primigenius*) from northern Germany. J. Quat. Sci. 24, 902–905.
Steinich, G., 1992. Die stratigraphische Einordnung der Rügen-Warmzeit. Z. Geol. Wiss. 20, 125–154.
Stephan, H.-J., 1995. Schleswig-Holstein. In: Benda, L. (Ed.), Das Quartär Norddeutschlands. Gebrüder Borntraeger, Berlin, pp. 1–22.
Stephan, H.-J., 2001. The Young Baltic advance in the western Baltic depression. Geol. Q. 45, 359–363.
Stephan, H.-J., Menke, B., 1977. Untersuchungen über den Verlauf der Weichselkaltseit in Schleswig-Holstein. Z. Geomorphol. N. F. 27, 12–28.
Stephan, H.-J., Kabel, C., Schlütler, G., 1983. Stratigraphical problems in the glacial deposits of Schleswig-Holstein. In: Ehlers, J. (Ed.), Glacial Deposits in North-West Europe. Balkema, Rotterdam, pp. 305–320.
Thomas, G.S.P., 1984. Sedimentation of a sub-aqueous esker-delta at Strabathie, Aberdeenshire. Scott. J. Geol. 20, 9–20.
Thomas, G.S.P., Connell, R.J., 1985. Iceberg drop, dump and grounding structures from Pleistocene glacio-lacustrine sediments, Scotland. J. Sediment. Petrol. 55, 243–249.
Tylmann, K., Piotrowski, J.A., Wysota, W., 2013. The ice/bed interface mosaic: deforming spots intervening with stable areas under the fringe of the Scandinavian Ice Sheet at Sampława, Poland. Boreas 42, 428–441.
Ukkonen, P., Aaris-Sørensen, K., Arppe, L., Clark, P.U., Daugnora, L., Lister, A.M., Lõugas, L., Seppä, H., Sommer, R.S., Stuart, A.J., Wojtal, P., Zupiņš, I., 2011. Woolly mammoth (*Mammuthus primigenius* Blum.) and its environment in northern Europe during the last glaciation. Quat. Sci. Rev. 30, 693–712.
van der Meer, J.J.M., 1996. Micromorphology. In: Menzies, J. (Ed.), Past Glacial Environments, Sediments, Forms and Techniques, Glacial Environments II. Butterworth-Heineman, Oxford, pp. 335–355.
van Rensbergen, P., de Batist, M., Beck, Ch, Chapron, E., 1999. High-resolution seismic stratigraphy of glacial to interglacial fill of a deep glacigenic lake: Lake Le Bourget, Northwestern Alps, France. Sediment. Geol. 128, 99–129.
Wiegank, F., 1972. Ökologische Analyse quartärer Foraminiferen. Beitrag zur Quartärstratigraphie in der nördlichen Deutschen Demokratischen Republik. Geologie 21, 1–111.
Winsemann, J., Asprion, U., Meyer, T., Schramm, C., 2007. Facies characteristics of Middle Pleistocene (Saalian) ice-marginal subaqueous fan and delta deposits, glacial Lake Leine, NW Germany. Sediment. Geol. 193, 105–129.
Winsemann, J., Hornung, J.J., Meinsen, J., Asprion, U., Polom, U., Brandes, C., Bußmann, M., Weber, C., 2009. Anatomy of a subaqueous ice-contact fan and delta complex, Middle Pleistocene, North-west Germany. Sedimentology 56, 1041–1076.
Wright, A.P., Siegert, M.J., 2011. The identification and physiographical setting of Antarctic subglacial lakes: an update based on recent advances. In: Siegert, M.J., Kennicutt, C., Bindschadler, B. (Eds.), Subglacial Antarctic Aquatic Environments. AGU Monograph.
Wysota, W., 2007. Successive subglacial depositional processes as interpreted from basal tills in the Lower Vistula valley (N Poland). Sediment. Geol. 193, 21–31.